2

On the search for non-noble based electrodes for oxygen reduction reaction

B. Viswanathan[1], Ch. Venkateswara Rao[1] and U. V. Varadaraju[2]
[1]Department of Chemistry, [2]Materials Science Research Centre
Indian Institute of Technology Madras, Chennai - 600 036, India

1. Introduction

The electrochemical reduction of molecular oxygen is important especially for devices such as metal air batteries (e.g., Zinc-Air batteries), fuel cells and air cathodes in many industrial electrocatalytic processes (e.g., chlor-alkali cells). Some of the important electrochemical devices are shown in Fig. 1. An understanding of oxygen reduction is important because it is often the counter electrode reaction that controls even the desired reaction process.

During the past decade, fuel cells received considerable attention from both energy and environmental stand points. Fuel cells appear to be one
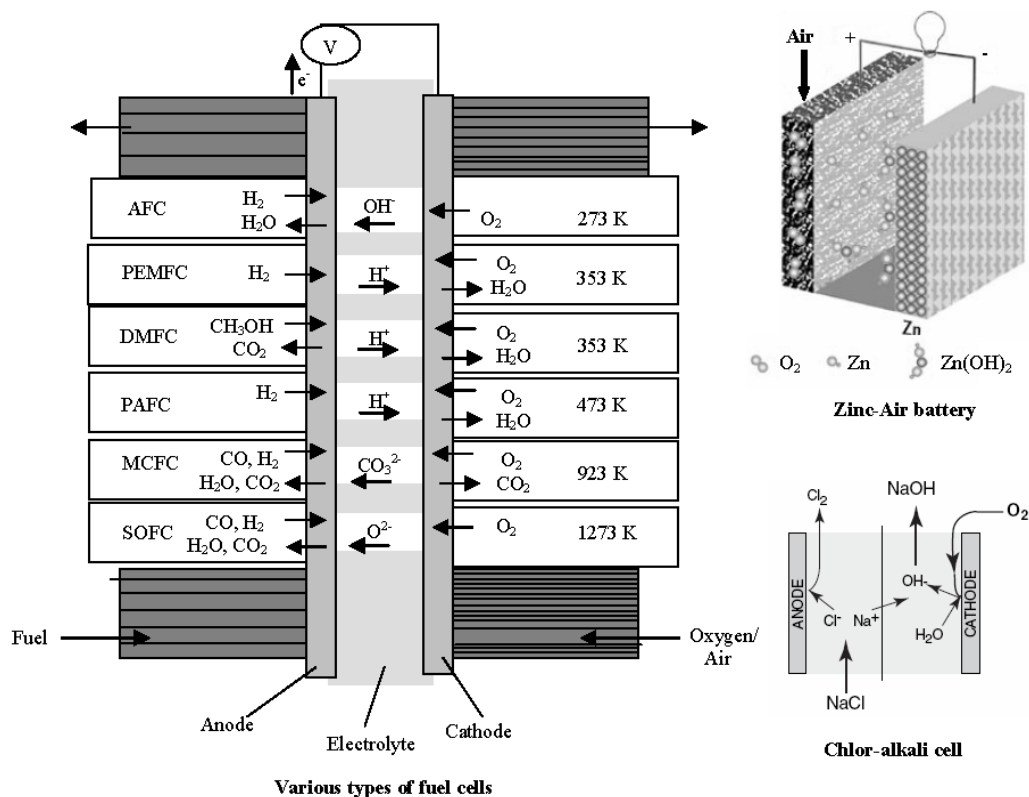
Correspondence/Reprint request: Dr. B. Viswanathan, Department of Chemistry, Indian Institute of Technology Madras, Chennai - 600 036, India. E-mail: bviswanathan@hotmail.com

Figure 1. Some of the important electrochemical devices [reproduced from ref. 3, 6 and 7].

of the alternate energy sources that can cater to the needs of future world. A fuel cell consists of an anode to which a fuel is supplied and a cathode to which an oxidant, commonly oxygen, is supplied. The oxygen needed by a fuel cell is generally supplied in the form of air. The two electrodes of a fuel cell are separated by an ion-conducting electrolyte. All fuel cells have similar basic operating principle. The input fuel is catalytically reacted (electrons removed from the fuel) in the fuel cell to create an electric current. The input fuel passes over the anode is catalytically split into electrons and ions. Oxygen passes over the cathode is reduced by the electrons which are generated at anode and passed on to the cathode by external circuit. At cathode, the ions which are formed at anode and transported to cathode, combine with the oxide ions and generate the oxidized product. If the fuel happens to be hydrogen, then water is formed [1, 2]. Depending on the input fuel and electrolyte, different chemical reactions will occur.

Among all batteries, because of its steady performance, source of raw material and low-cost, the study and development of Zinc–Air battery has received much attention. Because of their high specific energy (100 $Whkg^{-1}$) and environmentally benign materials, Zn–Air batteries are promising energy

storage devices. It is a special feature of the zinc–air system that only the active component of the negative electrode (zinc) needs to be stored in the battery, while the reactant for the positive electrode (oxygen) during discharge is drawn from air. This is the basis for the system's high specific energy—distinctly higher than that of conventional battery systems (Lead–Acid, Ni/Cd, and Ni/MH). The key problem in the development of Zn–Air batteries is the oxygen-diffusion electrode [3].

Industrial electrochemical processes such as the chlor-alkali process based on the electrolysis of brine for the production of chlorine and caustic soda is capital-intensive process. It also consumes significant power. This is true for today's existing process formulations, where chlorine is produced at the anode and NaOH and H_2 are obtained at the cathode. The hydrogen-evolving reaction has the penalty of working at a decomposition voltage of more than 1.2 V including the overvoltages and ohmic drops. Replacing the hydrogen-evolving cathode by an oxygen reduction (consuming) electrode in a membrane brine electrolysis cell reduces the total energy input to the cell by approximately 30% [4, 5]. Active electro catalysts are needed to reduce oxygen in order to get high cell efficiency. The characteristic features of various types of fuel cells, metal-air batteries and chlor-alkali cells are shown in Table 1.

Table 1. Characteristic features of various electrochemical devices.

Electrochemical device	Operating temp (K)	Electrolyte	Charge carrier	Electrolyte state	Oxidant for cell	Cathodic reaction
Alkaline fuel cell (AFC)	333-423	45% KOH	OH^-	Immobilized liquid	O_2/Air	$O_2 + 2\,H_2O + 4\,e^- \rightarrow 4\,OH^-$
Phosphoric acid fuel cell (PAFC)	453-493	H_3PO_4	H^+	,,	O_2/Air	$O_2 + 4\,H^+ + 4\,e^- \rightarrow 2\,H_2O$
Proton exchange membrane fuel cell (PEMFC)	333-353	Ion exchange membrane (e.g., Nafion)	H^+	Solid	O_2/Air	,,
Direct methanol fuel cell (DMFC)	333-353	,,	H^+	Solid	O_2/Air	,,
Molten carbonate fuel cell (MCFC)	923-973	Alkali carbonate mixture	CO_3^{2-}	Immobilized liquid	O_2/Air	$O_2 + 2CO_2 + 4e- \rightarrow 2CO_3^{2-}$
Solid oxide fuel cell (SOFC)	1073-1273	Yttria-stabilized zirconia	O^{2-}	Solid	O_2/Air	$O_2 + 4\,e^- \rightarrow 2\,O^{2-}$
Metal-air batteries (e.g., Zinc-air batteries)	298	Alkali	OH^-	Liquid	Air	$O_2 + 2H_2O + 4e^- \rightarrow 4OH^-$
Chlor-alkali cells	298	Alkali	OH^-	Liquid	Air	,,

Oxygen reduction reaction (ORR) has been studied over the years because of its fundamental complexity, great sensitivity to the electrode surface, and sluggish kinetics. The sluggish kinetics of ORR under the conditions employed in electrochemical devices is due to the low partial pressure of oxygen in air, slow flow rate of oxygen (i.e., less residence time for oxygen molecules on active sites) under ambient conditions. The main disadvantage in this important electrode reaction is the exchange current density (j_o) value in the region of 10^{-10} A/cm^2 in acidic medium and 10^{-8} A/cm^2 at 298 K in alkaline solution which is lower than the j_o value of anodic reaction (10^{-3} A/cm^2) in all the electrochemical devices [8]. Hence (from the equation $\eta = RT/nF \ln(j/j_o)$) the oxygen reduction reaction usually contributes considerably to the overpotential and therefore results in a low efficiency in the functioning electrochemical energy devices using air as oxidant. Understanding and exploitation of electrocatalysis for this reaction is needed more than any other reactions in electrochemical devices.

Figure 2 shows a typical voltage-current *(E* - I) discharge curve for a fuel cell with an open-circuit voltage E_{oc}. The overpotential $\eta = (E_{oc} - E)$ reflects the resistive IR losses due to the surface reaction kinetics, the resistance to transport of the working ion, H$^+$ or O^{2-} between the reductant and the oxidant reactive sites, and the resistance to diffusion of the oxidant and/or reductant to the catalytic sites and their products away from these sites. At low currents, the performance of a fuel cell is dominated by kinetic losses. These losses mainly stem from the high overpotential of the oxygen reduction reaction (ORR). At intermediate currents, ohmic losses arise from ionic losses in the electrodes and
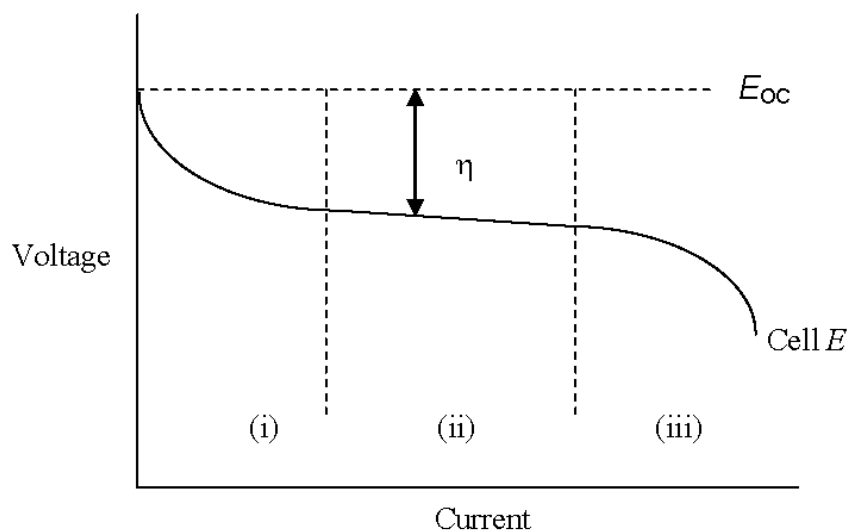

Figure 2. Typical polarization curve for a fuel cell: voltage drops due to: (i) surface reaction kinetics; (ii) electrolyte resistance; and (iii) reactant/product diffusion rates [reproduced from ref. 9].

and separator, although contact and electronic resistances can be important under certain operating conditions. At high currents, mass transport limitations become increasingly important. These losses are due to reactants not being able to reach the electrocatalytic sites. Typically, oxygen is the problem due to flooding of the cathode by liquid water, but protons and electrons can also cause mass-transfer limitations [9].

At any potential, both oxidation and reduction reactions can occur; at the rest potential φ_{oc}, the two reactions occur at equal rates. The net current density for an outer sphere reaction at a metallic electrode is given by the Butler-Volmer equation

$$j = j_o \left[\exp(\alpha_A nF\eta/RT) - \exp{-}(\alpha_C nF\eta/RT)\right]$$

where n is the number of electrons transferred in the reaction, F is the Faraday constant, η is the overpotential for the charge-transfer reaction at the surface, j_o is the exchange current density and α_A and α_C are the anodic and cathodic transfer coefficients respectively. For a concentration C_{ox} of the oxidizing species O_2 at the surface, the exchange current density of the cathodic ORR is

$$j_o = nFC_{ox}k_{ox}$$

where $k_{ox} = k_{0,ox} \, exp(-\Delta G(\varphi_{oc})/ RT)$ is the electrochemical rate constant and $\Delta G(\varphi_{oc})$ is the activation energy for electron transfer to the oxidant at the rest potential φ_{oc}. At small current densities, the exponents of the Butler-Volmer equation are small and the expansion of $exp(x)$ as $\sim 1+ x$ gives

$$j \sim j_o \, (nF \, \eta/RT) = \eta/R_{tr}$$

where the electron transfer resistance $R_{tr} = RT/j_o \, n \, F$ is independent of α_A and α_C. At low current densities ($i_o < 1$ mA cm^{-2}), electrodes gives a larger R_{tr} and therefore overpotential, η should be greater than 400 mV (at room temperature) [10]. An extremely active electrocatalyst is needed to overcome this initial voltage drop in the *E versus* current *discharge* curve.

To obtain a high performance cathode, a macroscopic dimensioning of the porous cathode layer has to be made with regard to cell design and to the composition of cathode materials. In general, oxygen reduction takes place at a three phase boundary (TPB). A gas diffusion electrode of high performance is required to reduce oxygen effectively at the cathode. The gas diffusion electrode should not only comprise of sufficient amount of electrode catalyst having low overvoltage for oxygen reduction reaction, but also should have a carrier on which highly dispersed electrocatalysts are supported. Moreover, the gas diffusion electrode should have a pore structure and hydrophobic nature of pore surface so as to enable the formation of a highly reactive three phase

boundary to form an interface where electrode catalyst, catholyte and oxygen contact effectively with each other. Its structure must satisfy two conflicting criteria, high gas permeability and low liquid permeability in order to achieve high performance required for commercial production [11-13]. Maintaining a stable interface between liquid and gas within the active layer of the gas-diffusion cathode is the key to long-term operation.

The essential criteria for a better cathode material are:

- high electronic conductivity
- high oxygen (or air) adsorption capacity
- chemical and structural stability under the conditions employed in devices i.e., operating temperature, wide range of oxygen partial pressure, concentration of electrolyte
- chemical and thermomechanical compatibility to electrolyte and interconnector materials
- high ionic (oxygen ion) conductivity
- ability to decompose the intermediate species formed during the reduction process
- tolerant to contaminants e.g., halide ions, methanol, NO_x, CO_x, SO_x
- low cost of materials

2. Mechanistic aspects of oxygen reduction

Even though oxygen reduction reaction (ORR) appears to be simple, it is quite complex. The molecular orbital diagram of oxygen molecule is shown in Fig. 3 [14]. According to Hund's rule, in the ground-state, O_2 possesses two unpaired electrons located in a doubly degenerate π^* antibonding orbital. This corresponds to a triplet state. The bonding orbitals of oxygen molecule can be ascribed to the $3\sigma_g$ orbital with two electrons, the doubly degenerate $1\pi_u$ and $1\pi_g^*$ orbitals, where the $1\pi_u$ orbital has double occupancy while the $1\pi_g^*$ orbital has single occupancy. The resulting bond order is two. When O_2 undergoes reduction, the electrons added occupy anti-bonding orbitals, decreasing the bond order of O-O. This increases the O-O bond distance and the vibrational frequency decreases. The excess of bonding over non-bonding electrons in the diagram of Fig. 3 is four. This explains the high stability of the O_2 molecule and its relatively low reactivity, in spite of its high oxidizing power [15].

The plausible 1:1 and 2:1 metal-dioxygen complex structures are given in Fig. 4. Geometries 1 and 2 have been shown to give similar bonding patterns: each exhibits one σ and one π interaction. The Griffiths model [16] **(1),** involves a side-on interaction of O_2 with the metal. The bonding can be viewed as arising from two contributions: σ type of bond formed by the overlap between a mainly π orbital of oxygen and d_z^2 (and s) orbital on the metal and a
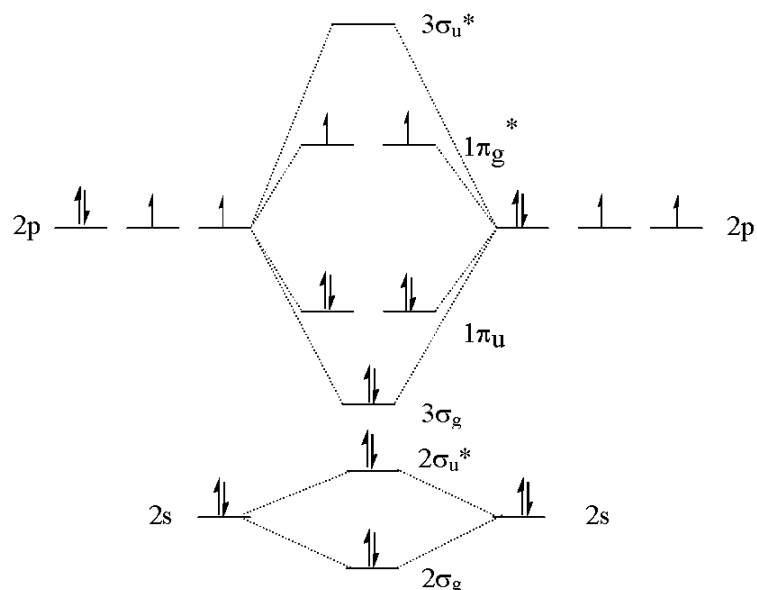
Figure 3. Molecular Orbital diagram of oxygen molecule [reproduced from ref. 14].
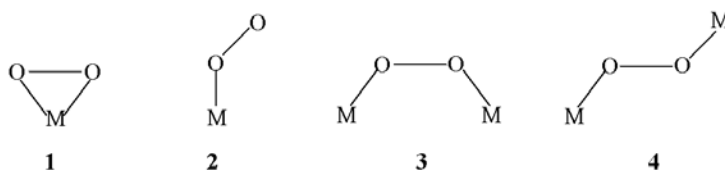

Figure 4. Possible configurations of dioxygen interaction with a metal in a complex.

π backbond interaction between the metal d π orbitals and the partially occupied π^* antibonding orbital on O_2. In the Pauling model [17] (**2**) which involves an end-on interaction of O_2 with the metal, a σ-bond is formed by the donation of electron density from the σ-rich orbital of dioxygen to an acceptor orbital d_z^2 on the metal whereas the π interaction is produced between the metal d-orbitals (d_{xz}, d_{yz}) and π^* orbital of dioxygen, with charge transfer from the metal to the O_2 molecule. It indicates that the preference of geometries (**1**) and (**2**) is determined by the relative donating abilities of the filled π and σ orbitals of dioxygen molecule respectively.

In 2:1 complexes of metal-dioxygen, the bonding arises from the interaction between the d-orbitals on the metal with π^* and π orbitals combination on O_2 [18]. It means that the singlet or triplet nature of dioxygen orbitals determines the bridge or trans mode of interaction of dioxygen with metal. The bridge interaction was proposed by Yeager [19] and it is likely to occur on noble metals such as Pt, face-to-face porphyrins [20] where O_2 is reduced to water with little or no peroxide formed. A trans configuration is likely to occur on metal porphyrins, metal phthalocyanines, dimeric metal

complexes [21, 22]. Griffith type of interaction could also lead to the rupture of the O-O bond. Some organometallic complexes [23] are known to form adducts with O_2 with a side-on interaction. However, these compounds do not exhibit any catalytic activity for O_2 reduction, probably because the interaction leads to a stable adduct. Depending on the mode of adsorption of oxygen molecule on metal surface, different mechanistic steps will occur [24-27]. The ORR pathways in both acidic and alkaline medium are given in Table 2.

Based on all these facts, various authors proposed different schemes for ORR pathway [28-30]. Of various schemes proposed for ORR, a modified scheme proposed by Wroblowa *et al.* [29] appears to be the appropriate one to describe the complicated reaction pathway for the reduction of O_2 at the metal surface (refer to Fig. 5).

At high potentials k_1/k_2 is constant with $k_1 > k_2$ indicating a direct reduction of oxygen to water than the two-electron reduction to peroxide. At intermediate potentials, k_1/k_2 ratio decreases indicating an increase in the two-electron reduction to peroxide. At lower potentials k_1/k_2 becomes lower than 1. However, k_3 increases resulting in a further reduction of peroxide to water before it escapes into solution.

On most of the electrocatalysts, oxygen reduction takes place by the formation of high energy intermediate, H_2O_2 followed by further reduction to H_2O. It is probably a consequence of the high stability of the O-O bond, which

Table 2. Mechanistic ORR pathways in acidic and basic media.

| Mode of interaction	ORR pathways	
	Acidic medium	Basic medium
Bridge (or) Trans	$O_2 + 2\,e^- + 2\,H^+ \rightarrow 2\,OH_{ads}$	$O_2 + 2\,e^- + 2\,H_2O \rightarrow 2\,OH_{ads} + 2\,OH^-$
	$2\,OH_{ads} + 2\,H^+ + 2\,e^- \rightarrow 2\,H_2O$	$2\,OH_{ads} + 2\,e^- \rightarrow 2\,OH^-$
	Overall direct reaction:	Overall direct reaction:
	$O_2 + 4\,H^+ + 4\,e^- \rightarrow 2\,H_2O$;	$O_2 + 2\,H_2O + 4\,e^- \rightarrow 4\,OH^-$;
	$E^o = 1.23$ V vs. NHE	$E^o = 0.401$ V vs. NHE
End-on	$O_2 + e^- + H^+ \rightarrow HO_{2,ads}$	$O_2 + H_2O + e^- \rightarrow HO_{2,ads} + OH^-$
	$HO_{2,ads} + e^- + H^+ \rightarrow H_2O$	$HO_{2,ads} + e^- \rightarrow HO_2^-$
	Overall indirect reaction:	Overall indirect reaction:
	$O_2 + 2\,H^+ + 2\,e^- \rightarrow H_2O_2$;	$O_2 + H_2O + 2\,e^- \rightarrow HO_2^- + OH^-$;
	$E^o = 0.682$ V vs. NHE	$E^o = -0.076$ V vs. NHE
	with $H_2O_2 + 2\,H^+ + 2\,e^- \rightarrow 2\,H_2O$;	with $HO_2^- + H_2O + 2\,e^- \rightarrow 3\,OH^-$;
	$E^o = 1.77$ V vs. NHE	$E^o = 0.88$ V vs. NHE
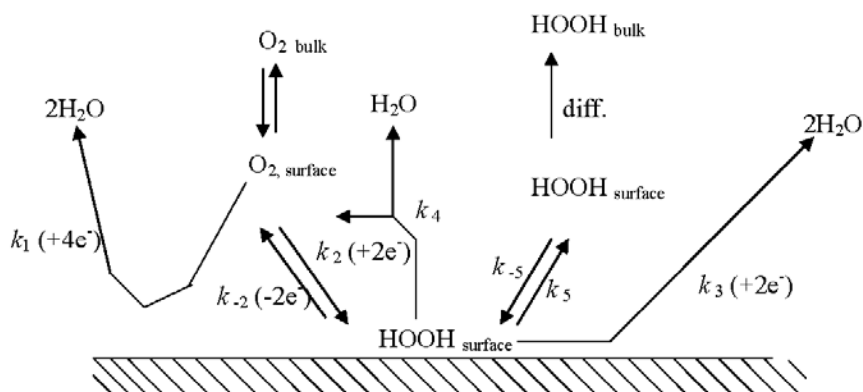
Figure 5. Schematic presentation of ORR pathway suggested by Wroblowa [reproduced from ref. 29]

has a dissociation energy of 494 kJ mol^{-1}. In contrast, the dissociation energy of the O-O bond in H_2O_2 is only 146 kJ mol^{-1} [31]. In order to obtain maximum efficiency and to avoid corrosion of carbon supports and other materials by peroxide, it is desired to achieve a four electron reduction. The two electron reduction is of practical interest for the production of hydrogen peroxide. Finding suitable electrocatalysts that can promote the direct four electron reduction of oxygen molecule is an important task.

3. Electrocatalysts for oxygen reduction

Both noble and non-noble metal based electrocatalysts were investigated for oxygen reduction. In the case of noble metal electrocatalysts, platinum based materials appear to be the best, whereas in the case of non-noble metal electro-catalysts several materials were investigated depending on the temperature of operation of electrochemical devices. Transition metal chalcogenides and pyrolyzed macrocyclic compounds are two of the most widely studied non-noble metal catalysts for oxygen reduction in electrochemical devices operated at low temperatures whereas transition metal oxides are employed in electrochemical devices operated at both low and high temperatures.

Oxygen reduction takes place at high positive potentials. At such potentials most of the metals will dissolve and give rise to a similar situation to that prevailing at the cathode i.e., only noble metals and some of their alloys offer possibilities among metallic systems. The most familiar oxygen reduction catalysts are based on noble metals, particularly platinum. These have been investigated extensively as pure metals, as nanoparticles [32] and alloys [33-35], and as polycrystalline and single crystal surfaces [36, 37]. They show a wide variety of behaviour, reflecting both the surface structure [38] and the presence or absence of oxide films [39]. To date, conventional carbon supported platinum based materials are the most active, efficient, applicable

and successful catalysts for electrochemical devices at the current technology stage. But the problem associated with this Pt catalysts is the slowness of ORR which is due to the formation of –OH species at +0.8 V, which inhibits further reduction of oxygen and hence results in loss of performance [40]. In order to compensate the loss of activity, one requires higher amounts of catalyst which dramatically increses the cost. However, there are several drawbacks to use Pt catalysts in fuel cells, beside the cost issue.

(1) Pt catalyzed oxygen reduction is not a complete four-electron reaction [41]. It is well known that the oxygen reduction reaction is a complex process that includes many electrochemical (chemical) steps with different intermediates. The hydrogen peroxide radicals produced by the two-electron reduction of O_2 can also attack the active sites and also carbon layer, resulting in significant degradation of electrochemical device, and even cause the failure of the device [42].
(2) Pt catalysts are sensitive to contaminants. For example, strongly adsorbing halides (i.e., Cl^-, Br^-, I^-) [43] and air borne contaminants of both organic (benzene, propane) [44] and inorganic (CO, NO_2, SO_2, NH_3, dust) [45-47] significantly reduce the activity of Pt catalysts in the operational potential range. While H_2O is the exclusive reaction product of the ORR on Pt at typical cathode potentials (0.6-1.0 V), the presence of strongly adsorbing halides changes the ORR pathway and substantial amounts of H_2O_2 are formed. This product degrades the Pt sites and it leads to the reduction in cell voltage and also its life span.
(3) Methanol contamination of the cathode catalyst, Pt, can occur through extensive cross-over in both DMFCs and in other fuel cells operating on incompletely reformed methanol. Problem is the development of mixed potential as a result of methanol oxidation and oxygen reduction at the cathode. Of these, the methanol oxidation current is little affected by the presence of oxygen, but the oxygen reduction current is suppressed by surface intermediates formed from the oxidation of methanol. This activity of cathode Pt towards methanol oxidation is not desirable. It leads to a drop in potential of the cathode, which lowers the operating cell voltage [48, 49].

So researchers focussed on alloys that prevents the adsorption of OH species, reduce oxygen selectively to water without being affected by the contaminants and tolerant to methanol. Among the alloys, Pt-Cr, Pt-Co and Pt-Fe shows higher activity for ORR and tolerence for methanol [34]. However, Pt alloys offer a performance gain of 25 mV, which increses the electrical efficiency of the fuel cell by 2%. This is the limit of the performance gain that can be expected using the approach of modifying the Pt face centred cubic lattice by alloying with base metals [50]. If much more of the 300 mV

available at the cathode is to be recovered, then a fundamentally different approach is required. The focus of the continued search for oxygen reduction catalysts should be on the development of materials with the required stability, and greater activity than Pt. Additionally, this will require that the electrocatalyst be prepared in a high surface area form to compete effectively with carbon supported platinum electrocatalysts. The focus of future research needs to be on improved performance.

There has been significant activity in recent years in electrochemistry of oxygen reduction to develop new and low-cost, non-noble metal-based electrocatalysts, which would be capable of selectively catalyzing the four-electron reduction of oxygen to produce water with low overpotential and low H_2O_2 production, a greater tolerance of contaminants, and the ability to remain inert during cathode methanol oxidation in direct methanol fuel cells.

4. Non-noble based electrocatalysts
4. 1. Transition metal oxides

Transition metal oxides, precisely because of their ability to switch between different valencies, possess appreciable chemical and/or electrocatalytic activity, which make them versatile materials for chemical and electrochemical reactions [51]. For the same reasons, these oxides exhibit remarkable stability toward chemical and electrochemical attack in appropriate conditions. Transition metal oxides, which can exist in various valency states, exhibit metal-like conductivity if half-filled d-bands are present. In other cases, due to the procedure of preparation, heavily non-stoichiometric oxides are obtained whose conductivity is only marginally lower than that of metals. These oxides can be used as electrodes even for practical applications, because the eventual ohmic drop across thin films is negligible. Many oxides have been investigated but it has been mainly focused on perovskites, spinels and pyrochlores since these materials can be expected to provide reversible pathway for oxygen reduction. To understand the electrochemical properties of these oxides, an additional interdisciplinary background of solid-state chemistry, surface chemistry, catalysis, and materials science is required. In general, oxide cathodes are of two types:

1) A porous, metallic oxide or a metallic oxide dispersed on or with carbon to form a porous metallic matrix. In this case, the oxide is catalytically active for the ORR (in the case of all electrochemical devices e.g., AFC, PAFC, PEMFC, DMFC, SOFC, MCFC, metal-air batteries and chlor-alkali cells). In this case, ORR occurs at a catalyst/electrolyte/air three phase linear interface.

2) A mixed electron/oxide-ion conductor that catalyzes the ORR is coated as a film on a solid oxide-ion electrolyte (in the case of SOFC and MCFC). In this case ORR occurs over the entire surface of the oxide film.

4.1.1. Bimetallic oxides

Alternate to platinum based catalysts, various simple metal oxides such as RuO_2, IrO_2, Fe_3O_4, PbO_2, NiO, $TiO_{2-\delta}$, CrO_2, PdO_x, CeO_2, ZrO_2, SnO_2, Ta_2O_5, $WO_{3-\delta}$ and MnO_2 [52-66] were investigated for oxygen reduction. Comparison of electrocatalytic activities towards oxygen reduction has led to the following order: RuO_2 and IrO_2>Co and Ni containing oxides>Fe, Pb and Mn containing oxides. MnO_2 shows some promise due to its low cost and its high catalytic activity for the oxygen reduction for metal-air battery applications [61, 67]. Even though these materials do not exhibit significant activity, the experience gained from the studies led to the search of new fascinating materials for oxygen reduction.

In MCFCs, the state-of-the-art cathode material is NiO lithiated *in situ* by Li^+ containing electrolyte [68]. However in the first long term performance tests of stacks, NiO turned out to be sufficiently soluble after several thousands rather than hundreds of hours. It is generally believed that acidic dissolution reaction occurs via the equilibrium $NiO + CO_2 \leftrightarrow Ni^{2+} + CO_3^{2-}$. Therefore, MCFC operation at high pressures is inevitably unfavourable for cathode stability [69]. There are three approaches to overcome this problem: the development of alternative cathode materials, the modifications of NiO with stable materials or with high lithium content and the modifications of the electrolyte with additives that stabilize the cathode dissolution. With regard to first approach, in 1990's, an extensive exploratory study of cathode materials was made by Argonne National Laboratories, which yielded $LiFeO_2$ and Li_2MnO_3 as prime candidates [70]. Later work elsewhere indicated that $LiCoO_2$ also shows much promise [71]. Li_2MnO_3 has the lowest solubility whereas $LiFeO_2$ has solubility comparable to that of NiO. Both are attractive because of low cost. Since their intrinsic activity is low, Makkus *et al.* [72] alleviated it by doping e.g., Mg for Mn in Li_2MnO_3, Mn or Co for Fe in $LiFeO_2$. However, the dopants tend to dissolve into the melt so that conductivity deteriorates (Mn-doped $LiFeO_2$), and they may collect unintentionally in other components. In this respect, $LiCoO_2$ is a better alternative but the material is costly. Cathodes made of $LiCoO_2$ perform equally as NiO, although this has been proved only in laboratory scale (3 cm^2). Concerning the second approach, Kuk *et al.* [73] applied a thin $LiCoO_2$ coated on the NiO particles of the cathode and reported a reduction in the NiO dissolution to 50%. NiO modified with CeO_2 [74], Nb_2O_5 [75], $LiFeO_2$ [76] and TiO_2 [77] has also been studied. About the third approach, the effect of the addition of alkaline earth oxide to the NiO cathode, such as MgO, CaO, SrO, BaO, SnO_2 and La_2O_3, have been investigated in various alkali carbonate electrolyte [78, 79]. These alkaline earth oxides contained in the cathodes are dissolved into the electrolyte under the cell operating conditions. The dissolution of alkaline earth oxide increases the basicity of the electrolyte and

then the solubility of NiO decreases. In spite of extensive research effort, lithiated NiO has remained the state-of-the-art cathode material. However, incremental improvements may not be sufficient to increase the lifetime of the cathodes in pressurized MCFC operation. To achieve a lifetime above 40000 h under these conditions and lower ohmic losses in the matrix will probably require $LiCoO_2$ or combined $NiO/LiCoO_2$ as cathode material. Of course, the cost of Co and the additional steps in the production process of a composite cathode such as $NiO/LiCoO_2$ remain as important obstacles.

4.1.2. Perovskites

The perovskite oxides have general formula ABO_3 in which A is the larger cation (+1 or +2) and B the smaller one (+4 or +5). The ideal structure is cubic with the A cation at the center of the cube 12 fold-coordinated with oxygen anions and the B cations occupying the corners of the cube in a 6-fold coordination, which is shown in Fig. 6. The great variety of properties that these compounds exhibit is due to the fact that 90% of the metallic elements in the periodic table can give stable perovskite type structures and also multicomponent oxides by partial substitution of cations in A and/or B positions [51].

Transition-metal metallic oxides with the perovskite structure contain basic cations like La^{3+} and/or an alkaline earth (i.e., their oxides have a point of zero zeta potential, pzzp at a pH > 7.0); oxides of these ions are not stable in strong acid solutions. Therefore, the study of perovskite metallic oxides as porous cathodes has been restricted to alkaline solution or to a solid oxide fuel cell operating at higher temperatures with an oxide ion solid electrolyte. Metal-Air batteries use an alkaline electrolyte; a rechargeable battery requires a bifunctional cathode active for both the ORR and OER (oxygen evolution reaction).
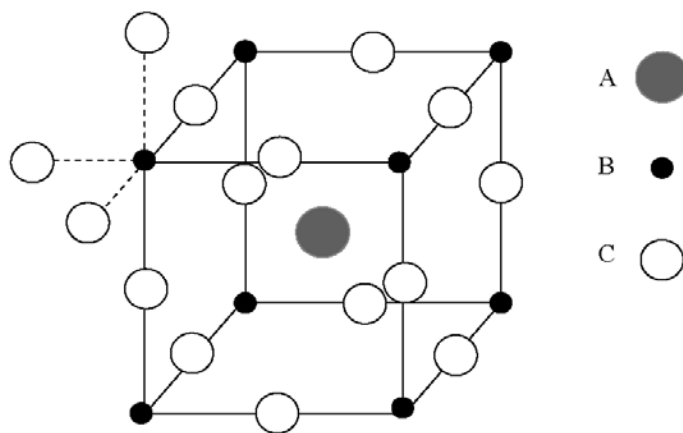

Figure 6. Ideal cubic perovskite [reproduced from ref. 51].

According to Goodenough [80], the feasibility of σ^* band formation between the e_g orbital of the transition metal ion and sp_σ of oxygen of the surface is an important factor in determining the electrocatalytic activity. Based on this concept, Matsumoto *et al.* [81] investigated the ORR activity of various metal oxides and observed better activity in $La_{1-x}Sr_xCoO_3$, $La_{1-x}Sr_xMnO_3$, $LaNi_{1-x}M_xO_3$ (M = Fe, Co) and Li doped NiO.

The more probable catalytic pathway of the ORR on an oxide in alkaline solution is the displacement to the solution of a surface OH^- species by $O_{2,ads}^-$, together with oxidation of a surface cation of the catalyst to form a surface peroxide species O_2^{2-}. This reaction can occur where the surface-cation redox couple is such that the reduced cation attracts a proton from the solution to its surface O^{2-} ion ligand in the operating alkaline solution and the more acidic oxidized cation repels the surface proton to the solution. The accessible transition-metal redox couples of perovskites that give a highly deprotonated oxidized surface and protonated reduced surface in alkaline solution appear to include M(IV)/M(III) couples of Cr, Mn, Fe, Co, and Ni. However, studies were mostly concentrated on perovskites operating on the Mn(IV)/Mn(III) and Co(IV)/Co(III) couples as these provide better electronic conductivity and chemical stability.

Various perovskites, ABO_3 (A = La, Ca, or Sr, and B = Co, Fe, Cr or Mn) were tested in the search for a cathode material for electrochemical devices in alkaline electrolyte. Among these, cobaltites were catalytically active but unstable chemically under cathodic conditions in a concentrated alkaline solution. Muller *et al.* [82] obtained the polarization curves of high-surface area $La_{0.6}Co_{0.4}O_{3-\delta}$ perovskite homogeneously dispersed at 20% loading on corrosion resistant, graphitized Vulcan XC72R carbon powder in 45% KOH. It acts as a powerful bifunctional air electrode in 45% KOH. Catalyst dissolution due to erosion of the active surface by oxygen evolution and partial destruction of the electrode morphology limited the cycle life to about 1400 h of cathodic-anodic cycling. In contrast, the ferrites were stable but hardly active. Only, manganites were active and stable, showing promise. Hyodo *et al.* [83] examined a series of manganites, $LnMnO_3$ (Ln = lanthanides and Y) for their electrocatalytic activities to reduce oxygen in alkaline solution. Polarization experiments using gas diffusion electrodes revealed that the catalytic activity differed significantly in the order of La>Pr>Nd>Sm>Gd>Y>Dy>Yb. For DMFC applications, Karthik *et al.* [84] tested the performance of the carbon supported perovskites $LaMO_3$ (M = Fe, Co, Ni, Mn) in 2.5 M H_2SO_4 and 3.0 M KOH solutions containing 3.0 M CH_3OH. $La_{0.9}Sr_{0.1}NiO_3$ and $La_{0.8}Sr_{0.2}CoO_3$ possess adequate stability and higher activity for the cathodic reduction of oxygen in alkaline solutions. An overvoltage of 200 mV at 100 mA/cm^2 is reported. Miura *et al.* [85] investigated the ORR activity of PTFE-bonded C electrodes loaded with $La_{0.6}Sr_{0.4}Fe_{0.6}M_{0.4}O_3$ and $La_{0.8}Sr_{0.2}MO_3$ (M = Mn, Co).

The highest cathode performance was achieved with the electrode containing 40 wt% $La_{0.5}Sr_{0.4}Fe_{0.6}Co_{0.4}O_3$; the current density as high as 1600 mA/cm^2 was obtained at 0.65 V vs. NHE in 9 M NaOH at 353 K. The ability to decompose HO_2^- was considered to be necessary to obtain high current densities because under such a strongly polarized electrode potential, HO_2^- can easily be produced on C substrate or on catalysts themselves. The electrode activity was stable over a short term operation of 50 h at the current density of 300 mA/cm^2. Recently, Yuasa *et al.* [86] prepared $La_{1-x}Sr_xMn_{0.8}Fe_{0.2}O_{3+\delta}$ (x = 0 - 0.4) and $La_{0.8}Sr_{0.2}Mn_{1-y}Fe_yO_{3+\delta}$ (y = 0 - 0.8) supported on C by a reverse micelle method. The highest activity measured is 500 mA/cm^2 at 0.7 V vs. NHE in 9 M NaOH at 358 K under O_2 flow, was that of the oxides with x = 0.4 and y = 0.2. A loading of 17% of $La_{0.6}Sr_{0.4}Mn_{0.8}Fe_{0.2}O_{3+\delta}$ on an electrode was compared with a 27.7% Pt-loaded electrode for oxygen reduction activity. The 17%-loaded electrode was better than the Pt-loaded electrode.

Cathode materials for SOFC applications can be divided into two groups: (1) electronic conductors (EC) such as metals and some metal oxides; and (2) mixed ionic-electronic conductors (MIEC) which are exclusively metal oxides. In EC cathodes, the oxygen has to be transported in the gas phase or as an adsorbed species along the surface of the porous electrode structure (surface diffusion). Assuming an ideal electrolyte material with negligible electronic conductivity, the incorporation of oxygen into the electrolyte is restricted to the three phase boundaries (TPB). Therefore, the polarization resistance is directly connected to the electrode microstructure, i.e., the arrangement of the TPB. In MIEC cathodes' oxygen ions can also be transported through the bulk of the cathode material to the electrolyte interface (Fig. 7). The polarization resistance is then related to the diffusion coefficient D of oxide ions, the surface exchange coefficient of the electrode and to the resistance for the transfer from the cathode material to the electrolyte. Especially at decreased
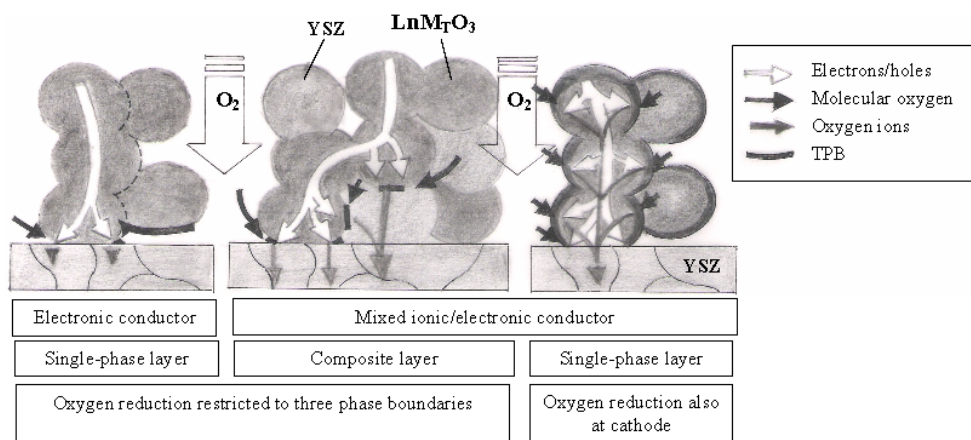

Figure 7. Types of electronic and conducting cathodes [reproduced from ref. 87].

operating temperatures (773 - 973 K) MIEC cathodes offer significant advantages, whereas at high operating temperatures problems due to interdiffusion and densification affect the long-term stability. Regarding the basic requirements of a cathode material for SOFCs, many perovskite systems $La_{2-x}A_xMO_3$, where A = Sr, Ca and B = Cr, Mn, Co, Fe, Ni were tested. Among these multicomponent oxide systems, (La, Sr)CoO_3 (LSC) and (La, Sr)MnO_3 (LSM) meet the requirements of cathode material for SOFC. Herbstritt *et al.* [88] investigated the ORR activity in single cell mode with different types of cathode materials and achieved similar performance in the case of screen printed LSC and LSM at power densities < 250 mWcm^{-2}. It should be noted that screen printed LSC cathodes showed a significant degradation during the first hundred hours of operation. Because of the high thermal expansion coefficient of (La,Sr)CoO_3, it cannot be used. On the other hand, this material exhibits an insufficient chemical compatibility to zirconia based electrolytes. Compared to LSM, the formation of secondary phases (lanthanum and strontium zirconates) at the LSC/YSZ interface occurs on a larger scale [89]. Therefore the oxygen ion transport in the cathode material is hindered due to the transfer resistance between the cathode and the electrolyte. At present, the state-of-the-art cathode material in SOFCs is $La_{2-x}Sr_xMnO_3$ (x = 0.15-0.25).

4.1.3. Spinels

The metal oxides having the composition AB_2O_4 are called spinels. In the ideal structure, shown in Fig. 8, oxide ions form an fcc packing, while the A and B cations are located in the octahedral and tetrahedral sites [51]. A specific feature of the crystalline structure of all spinels is that the crystallographically equivalent places in the lattice are occupied by cations of different valencies, between which electronic transitions take place without perceptible energy.

Spinels such as Co_3O_4 [91], $NiCo_2O_4$ [92], $CoFe_2O_4$ [93], and $MnCo_2O_4$ [94] have been investigated for oxygen reduction. These materials are also restricted to alkaline medium as they undergo leaching in acid medium. In order to increase the stability, Nguyen-Cong *et al.* [95] used conducting polymer polypyrrole (PPy) layers to protect the dissolution of metal oxide ($Ni_{0.3}Co_{2.7}O_4$). Both the oxide and PPy were electrodeposited onto carbon electrodes in such a fashion that the oxide is sandwiched between PPy layers. A remarkable electrochemical stability of the oxide at acidic conditions is achieved. Also interesting observation is that the electrical conductivity of the composite film is retained at potentials at which PPy is usually in an insulator state. The effect of the counter ions in the composite is the area of research that is continued even today. It is believed that electrical conductivity is directly related to the electropolymerization processes. Counter anions have a profound effect on the polymerization process and the resulting composites demonstrate
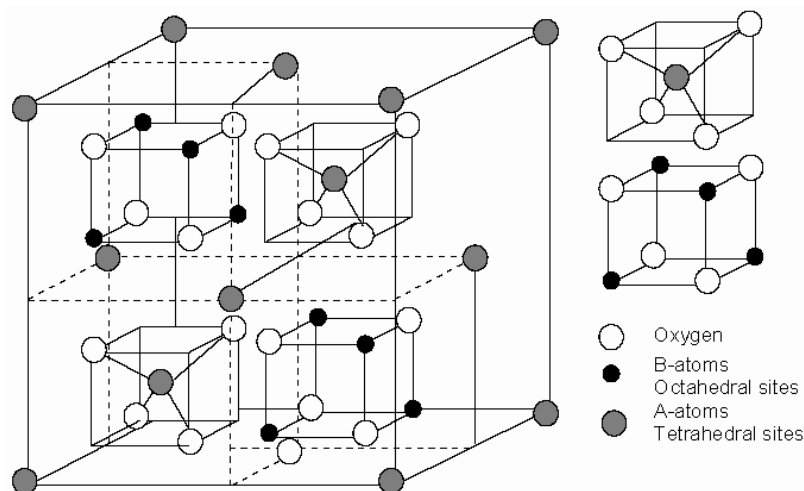
Figure 8. AB_2O_4 Spinel structure [reproduced from ref. 90].

characteristic ORR activities. A similar study utilized $CoFe_2O_4$ and PPy to form sandwiched composites [96]. The electrode exhibits high electrocatalytic activity towards oxygen reduction and stability in acidic media and at high cathodic potentials. Metal oxide nanoparticles embedded in a conductive polymer matrix seem to be a promising design for ORR electrode.

Among the spinel systems, $NiCo_2O_4$ is the best but the activity and stability were lower compared to perovskites. King and Tseung [97] studied the reduction of O_2 on $NiCo_2O_4$ and found that it possessed high activity for the reduction of oxygen (250 mA/cm^2 at 0.65 V, 5 N KOH, 298 K). However, the performance decreased to less than 2 mA/cm^2 within 2-3 hr. In order to increase the performance, Tseung and Yeung [98] investigated the activity in oxygen saturated KOH (5 N) by binding $NiCo_2O_4$ with Teflon and observed 25 mA/cm^2 at 750 mV over a test period of 130 hr. Recently, Nissinen *et al.* [94] synthesized $MnCo_2O_4$ supported on carbon by microwave assisted method and observed ORR activity of 12 mA/cm^2 at 650 mV in 6 N KOH.

4.1.4. Pyrochlores

The face centered oxide pyrochlore structure [99] can crystallographically best be described by the general formula: $A_2M_2O_6O'$ where A = Pb or Bi, B = Ru or Ir, $0<x<1$ and $0<y<0.5$ contains a cubic M_2O_6 framework of corner-shared octahedra that is interconnected by an A_2O' array which is shown in Fig. 9. The framework has its M-O-M bond angle buckled from 180° to about 135°. The strong M-O-M interactions within the M_2O_6 framework are responsible for the metallic conductivity of pyrochlore oxides. The O' sites are tetrahedrally coordinated to A cations whereas the O sites are coordinated to two A and two M cations. These special oxygens (O') may be partially or totally absent and are the basis for the anion non-stoichiometry observed in pyrochlores.
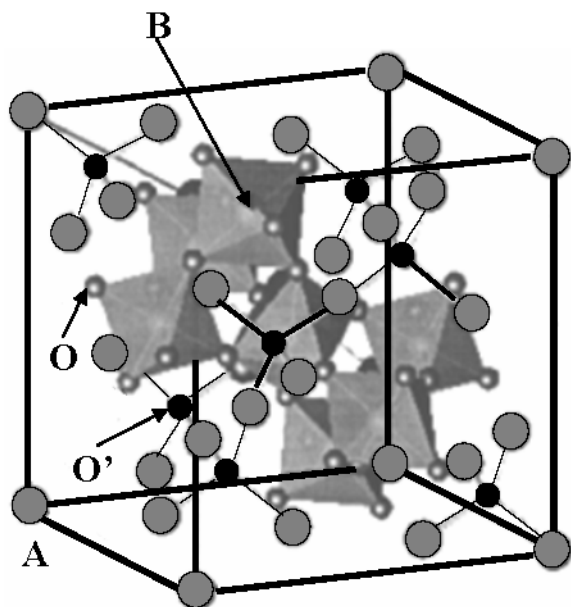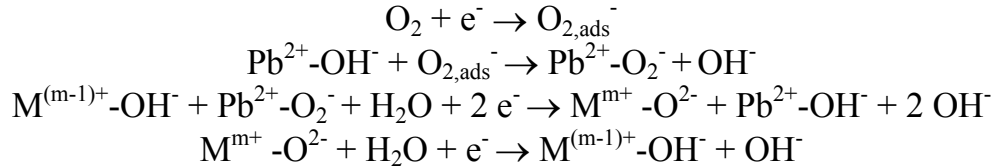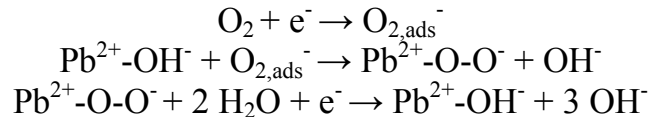
Figure 9. The M_2O_6 array of cubic $A_2M_2O_6O'$ pyrochlore (A_2O' array occupies intersecting interstitial channels) [reproduced from ref. 99].

The Pb-Ru pyrochlore was first identified by Horowitz *et al.* [100] as an active electrocatalyst for oxygen reduction whose efficiency was considered to be comparable to that of the noble metals in alkaline medium. This material is also known to be stable in acids. The presence of a Ru^{+5}/Ru^{+4} redox couple between the potentials for the OER and ORR and $Ru-O_b-Ru$ interactions strong enough to make the oxide metallic appear to play critical roles in rendering the ruthenium oxides active for these reactions. Early studies of the electrocatalytic activity of the pyrochlores $A_2[A_xRu_{2-x}]O_6O'_{1-y}$ with A = Pb or Bi showed that these oxides catalyze the ORR in both acid and alkaline environments [101, 102]. The substitution of the larger Pb^{4+} (0.775 Å) or Bi^{4+} (0.72 Å) for Ru^{4+} (0.62 Å) on the octahedral coordinated Ru-site leads to a considerable enlargement of the pyrochlores unit cell dimension in such a way that the feasibility of the displacement of OH^- ions by O^{2-} (rate determining step for the ORR) is predominant. It means that the M-site Ru atoms control the delivery of electrons to the surface and hence to the reaction sites. Under the conditions employed in electrochemical devices, erosion of the oxide catalyst with O_2 evolution and partial destruction of the electrode morphology take place on repeated cathodic-anodic cycling which causes the diffusion of ruthenates and plumbates out of the electrode. The enhancement in the activity and stability was observed when it was dispersed on the carbon support and/or conducting polymer. The polarization curves obtained by Horowitz *et al.* [103] for the ORR in 3 M KOH at 75 ^{o}C showed comparable activity for $Pb_2[Pb_{0.58}Ru_{1.42}]O_6O'_{0.5}$ dispersed on carbon with that on 15 wt.% Pt dispersed

on carbon. Moreover, they observed negligible amount of hydrogen peroxide intermediates, which suggests that either the O' vacancies promote the equation (4) of the reaction mechanism given in subsequent sections, as the reaction pathway or offer, as an alternative, the following pathway:

$$O_2 + e^- \rightarrow O_{2,ads}^-$$
$$Pb^{2+}\text{-}OH^- + O_{2,ads}^- \rightarrow Pb^{2+}\text{-}O_2^- + OH^-$$
$$M^{(m-1)+}\text{-}OH^- + Pb^{2+}\text{-}O_2^- + H_2O + 2\ e^- \rightarrow M^{m+}\text{-}O^{2-} + Pb^{2+}\text{-}OH^- + 2\ OH^-$$
$$M^{m+}\text{-}O^{2-} + H_2O + e^- \rightarrow M^{(m-1)+}\text{-}OH^- + OH^-$$

In 1989, Manoharan $et\ al.$ [104] observed slightly increased ORR activity by substitution of Ir for Ru in $Pb_2[Pb_xIr_{2-x}]O_6O'_{1-y}$. They investigated the ORR activity in both acidic and alkaline conditions by binding the particles to one another and to a Pt screen current collector with Teflon without the presence of carbon. Excellent activity for the ORR in an alkaline metal/air battery or alkaline H_2/air fuel cell was observed whereas poor activity was observed in H_2SO_4. Since the performance of an electrode depends on the number of active sites present on the surface, Raghuveer $et\ al.$ [105] prepared nanocrystalline $Pb_2Ru_{1.95}\ Pb_{0.05}\ O_{7-\delta}$ by reverse micellar method and sol-gel method and observed higher activity than that of commercial platinum catalyst under acidic conditions. Measurements of surface charge of the oxide particles against pH revealed that protonation of Ru_2O_6 occurs to form $Ru^{3+}\text{-}OH^-$ under acidic conditions whereas the reverse situation prevails in basic conditions [106]. In 2.5 M H_2SO_4, a pH < pzzp ensures that all O' sites contain fully protonated water molecules. Therefore these sites would not be active for ORR according to equation (2), shown in reaction scheme given subsequently. So the active sites for the oxygen reduction are OH^- species at the O-site positions (Ru_2O_6) of the pyrochlores. The reaction follows steps (1) and (2) of the reaction scheme. In 1 M NaOH, a pH > pzzp implies that the O' sites are occupied by OH^- ions and there is no protonation of the Ru_2O_6 array. Consequently the ORR proceeds on the Pb^{2+} ions and O' sites:

$$O_2 + e^- \rightarrow O_{2,ads}^-$$
$$Pb^{2+}\text{-}OH^- + O_{2,ads}^- \rightarrow Pb^{2+}\text{-}O\text{-}O^- + OH^-$$
$$Pb^{2+}\text{-}O\text{-}O^- + 2\ H_2O + e^- \rightarrow Pb^{2+}\text{-}OH^- + 3\ OH^-$$

4.1.5. ORR mechanism
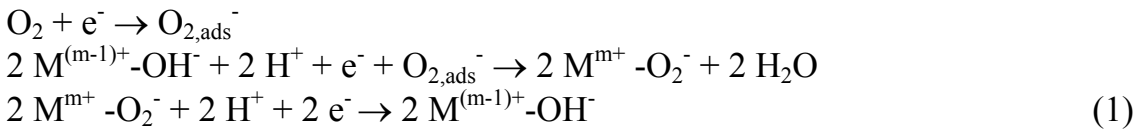
In general, oxygen reduction takes place at three phase interface (O_2 or air/electrolyte/metal oxide). Understanding the processes at three interfaces is difficult because of the inter dependence of parameters associated in each phase. So the mechanism at two phase interface which gives reasonable information can be extended for the three phase interface. Tarasevich [107] and Trunov [108]

have discussed the mechanism of oxygen reduction on metal oxides. Fractional orders have been observed, which point out to the importance of surface hydration in all aspects of the electrochemical behaviour of oxides.
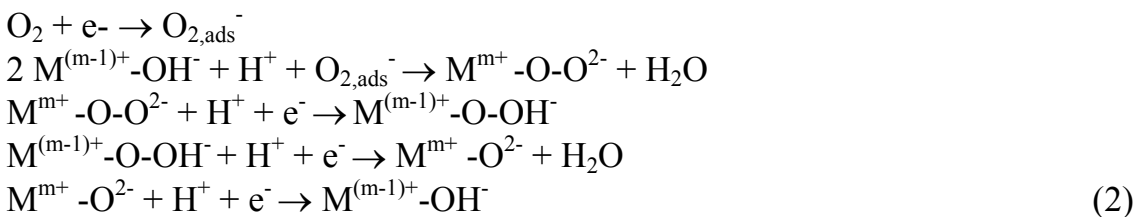
Metallic oxide/aqueous electrolyte interface

The ORR pathway at the surface of a metallic oxide takes place in the similar way as that of metals but with a modified charge distribution. In vacuum, oxide surfaces expose two main sites: metal and oxide ions. Oxide surfaces are reactive toward water in the gas phase, especially because of the strong Lewis acidity of metal ions. As oxides are brought in contact with an aqueous solution, the surface will become covered by OH groups (protons are from water molecules) whose concentration will depend on the nature of the oxide and its specific crystal surface. The OH groups on the surface of oxides in aqueous solution behave as weak acids or bases. Accordingly the ORR pathways involve exchange of surface protons and displacements of surface species by equally charged adsorbed molecules. The pH of zero zeta potential (pzzp) of an oxide ion is therefore, an important determinant of the pH at which an oxide is active for the ORR. At pzzp, the oxide particles have no charge. At pH < pzzp, the surface accepts protons from the solution and the particles become positively charged; at a pH > pzzp, the bound water at the oxide surface donates protons to the solution and the particles become negatively charged. A particle is said to be acidic if it has a pzzp < 7.0, or to be basic if it has a pzzp > 7.0 [106]. The electrochemical potential across the interface between a metallic oxide and an aqueous electrolyte is kept constant by the electric field established across the Helmholtz double layer to the liquid. Consequently, reduction of a surface cation by an electron from the external circuit is charge-compensated by protonation of a surface oxygen ligand.
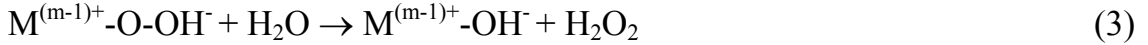
Based on the above concepts, the ORR pathways can be envisaged in acid solution as

$$O_2 + e^- \rightarrow O_{2,ads}^-$$
$$2\ M^{(m-1)+}\text{-}OH^- + 2\ H^+ + e^- + O_{2,ads}^- \rightarrow 2\ M^{m+}\text{-}O_2^- + 2\ H_2O$$
$$2\ M^{m+}\text{-}O_2^- + 2\ H^+ + 2\ e^- \rightarrow 2\ M^{(m-1)+}\text{-}OH^- \qquad (1)$$

Provided the oxygen molecule displays two adjacent surface OH^- anions or, more probably,

$$O_2 + e\text{-} \rightarrow O_{2,ads}^-$$
$$2\ M^{(m-1)+}\text{-}OH^- + H^+ + O_{2,ads}^- \rightarrow M^{m+}\text{-}O\text{-}O^{2-} + H_2O$$
$$M^{m+}\text{-}O\text{-}O^{2-} + H^+ + e^- \rightarrow M^{(m-1)+}\text{-}O\text{-}OH^-$$
$$M^{(m-1)+}\text{-}O\text{-}OH^- + H^+ + e^- \rightarrow M^{m+}\text{-}O^{2-} + H_2O$$
$$M^{m+}\text{-}O^{2-} + H^+ + e^- \rightarrow M^{(m-1)+}\text{-}OH^- \qquad (2)$$

with competition from the reaction

$$M^{(m-1)+}\text{-O-OH}^- + H_2O \rightarrow M^{(m-1)+}\text{-OH}^- + H_2O_2 \tag{3}$$

In alkaline solution, the corresponding pathways should be

$$2\,M^{m+}\text{-O}^{2-} + H_2O + e^- \rightarrow M^{(m-1)+}\text{-OH}^- + 2\,OH^-$$
$$O_2 + e^- \rightarrow O_{2,ads}^-$$
$$M^{(m-1)+}\text{-OH}^- + O_{2,ads}^- + e^- \rightarrow 2\,M^{m+}\text{-O}^{2-} + 2\,OH^- \tag{4}$$

or more probably

$$M^{m+}\text{-O}^{2-} + H_2O + e^- \rightarrow M^{(m-1)+}\text{-OH}^- + OH^-$$
$$O_2 + e^- \rightarrow O_{2,ads}^-$$
$$M^{(m-1)+}\text{-OH}^- + O_{2,ads}^- \rightarrow M^{m+}\text{-O-O}^{2-} + OH^-$$
$$M^{m+}\text{-O-O}^{2-} + H_2O + e^- \rightarrow M^{(m-1)+}\text{-O-OH}^- + OH^-$$
$$M^{(m-1)+}\text{-O-OH}^- + e^- \rightarrow M^{m+}\text{-O}^{2-} + OH^- \tag{5}$$

with competition from the reaction

$$M^{m+}\text{-O-O}^{2-} + H_2O + e^- \rightarrow M^{(m-1)+}\text{-OH}^- + HO^{2-} \tag{6}$$
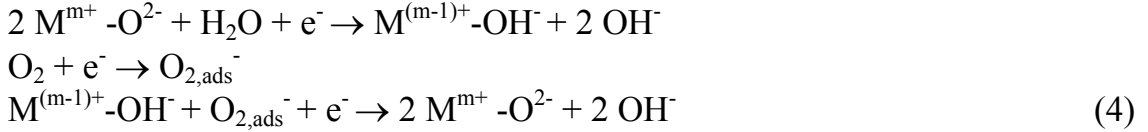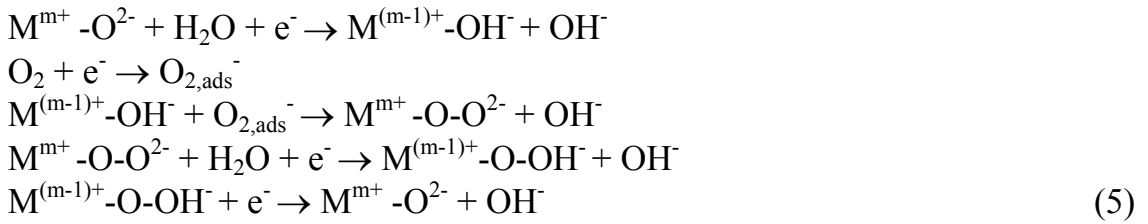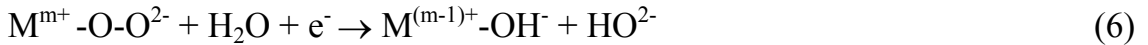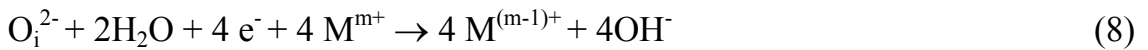
An alternative approach would be the use of an oxide that accepts interstitial oxygen, O_i at room temperature in air atmosphere. In this case, the reaction pathway would be

$$4\,M^{(m-1)+} + O_2 \rightarrow M^{m+} + 2\,O_i^{2-}$$
$$O_i^{2-} + 4\,H^+ + 4\,e^- + 4\,M^{m+} \rightarrow 4\,M^{(m-1)+} + 2H_2O \tag{7}$$

or

$$O_i^{2-} + 2H_2O + 4\,e^- + 4\,M^{m+} \rightarrow 4\,M^{(m-1)+} + 4OH^- \tag{8}$$
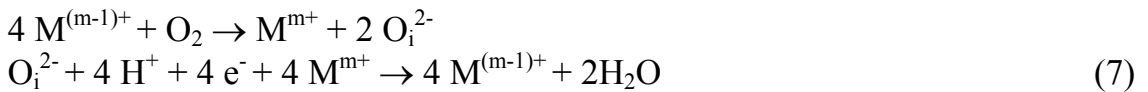
**Metallic oxide/air interface**

The ORR at a metallic oxide/air interface occurs at the cathode of a solid oxide fuel cell or the air side of a permeation membrane. In these applications, the oxide may be a mixed ion/electronic conductor and the operating temperature is > 873 K. At high operating temperature, the bound water is evaporated from the surface of the oxide and the product of the reduction of O_2 is $2O^{2-}$. The O^{2-} ions are removed from the catalytic surface by diffusion from the oxidizing atmosphere toward a reducing atmosphere at the opposite side of the MIEC film or membrane. In a fuel cell, the cathode need not be a MIEC. Where the metallic oxide is not an oxide ion conductor, the oxide ions spill over from the catalyst to the electrolyte at a three-phase catalyst/electrolyte/air

interface [9]. Loss of bound water from the surface of an oxide creates surface cations with missing oxide ion ligands that can be attacked by a gaseous O_2 molecule. However, if the surface reconstructs, attack of the surface by gaseous O_2 requires activation energy.
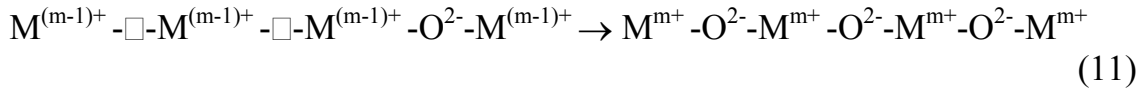
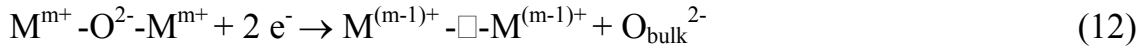The ORR at an oxygen vacancy proceeds by the pathway

$$M^{(m-1)+} \text{-}\square\text{-}M^{(m-1)+} + O_2 \rightarrow M^{m+} \text{-}(O_2)^{2-}\text{-}M^{m+} \tag{9}$$

and the extra, active oxygen of the O_2^{2-} anion migrates over the surface to another vacancy where it is reduced:

$$O_{ads} + M^{(m-1)+} \text{-}\square\text{-}M^{(m-1)+} \rightarrow M^{m+} \text{-}O^{2-}\text{-}M^{m+} \tag{10}$$
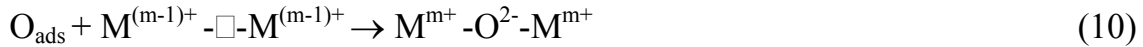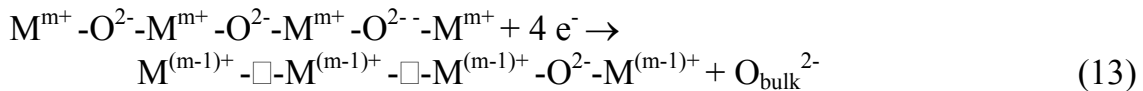
unless it first meets another active oxygen with which it recombines to form gaseous O_2. Alternatively, an O_2 molecule may attack a surface cation in tetrahedral coordination to transform it to octahedral coordination in the direct ORR

$$M^{(m-1)+} \text{-}\square\text{-}M^{(m-1)+} \text{-}\square\text{-}M^{(m-1)+} \text{-}O^{2-}\text{-}M^{(m-1)+} \rightarrow M^{m+} \text{-}O^{2-}\text{-}M^{m+} \text{-}O^{2-}\text{-}M^{m+} \text{-}O^{2-}\text{-}M^{m+} \tag{11}$$

As the oxide ions diffuse away from the oxidizing atmosphere towards the reducing atmosphere, the charge at the catalytic surface is kept constant by the diffusion of electrons in the opposite direction:

$$M^{m+} \text{-}O^{2-}\text{-}M^{m+} + 2 \text{ e}^- \rightarrow M^{(m-1)+} \text{-}\square\text{-}M^{(m-1)+} + O_{bulk}^{2-} \tag{12}$$

or alternatively

$$M^{m+} \text{-}O^{2-}\text{-}M^{m+} \text{-}O^{2-}\text{-}M^{m+} \text{-}O^{2-}\text{-}M^{m+} + 4 \text{ e}^- \rightarrow$$
$$M^{(m-1)+} \text{-}\square\text{-}M^{(m-1)+} \text{-}\square\text{-}M^{(m-1)+} \text{-}O^{2-}\text{-}M^{(m-1)+} + O_{bulk}^{2-} \tag{13}$$

The rate limiting step of the overall reaction on an MIEC film or membrane may be either initial ORR at the surface or the rate of the O^{2-} ions away from the surface. The rate of diffusion increases with the difference in the oxygen activity on opposite sides of the MIEC and as the thickness of the MIEC film or membrane is decreased at a critical thickness, the rate of the ORR is controlled by both the surface reaction kinetics and the rate of oxide ion diffusion away from the surface.

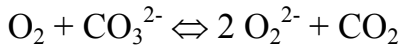However, if a Pt catalyst is used, the reaction follows the following steps

$$O_2 + \text{e}^- \rightarrow O_{2,ads}^-$$
$$2 \text{ } O_{2,ads}^- + 2 \text{ e}^- + 2 \text{ } \square_{el} \rightarrow 2 \text{ } O_{el}^{2-} \tag{14}$$

where O_{ads}^- is adsorbed on the Pt from where it spills over to a vacancy $\square_{el}$ in the electrolyte as O_{el}^{2-}.

**Oxygen reduction on an oxide-ion electrolyte**

Oxygen reduction at the electrolyte/air interface can occur at a three phase metal/ electrolyte/air interface. Oxygen may be adsorbed either as an oxygen molecule in an oxygen vacancy of the electrolyte, or on the metal. In the former case, electrons from the metal reduce the oxygen molecule to the peroxide ion; one oxygen of the peroxide migrates into the surface vacancy, and accepts two electrons from the metal. Alternatively, the adsorbed oxygen on the catalytic metal as $2O_{ads}^-$ spills over into electrolyte surface vacancies as an oxide ion as described in equation (14). The ORR at the cathode balances the loss of oxide ions at the anode whereas electrons are given to the metal electrode as the surface oxygen reacts either with one another to form O_2 gas or with fuel to form, for example, H_2O and/or CO_2.

In view of the complex nature of carbonate melts, many mechanisms have been proposed for the oxygen reduction, and that a definitive answer still eludes us, especially with respect to the reaction process in an actual MCFC cathode [9]. The most acceptable route is the mechanism proposed by Appleby and Nicholson [109-111] based on half cell studies in various eutectic melts. According to them, the reaction takes place in either peroxide pathway or superoxide patheway.
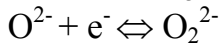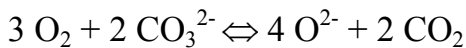
Peroxide pathway

$$O_2 + CO_3^{2-} \Leftrightarrow 2\ O_2^{2-} + CO_2$$
$$O_2^{2-} + 2\ e^- \Leftrightarrow 2\ O^{2-} \tag{15}$$
$$O^{2-} + CO_2 \Leftrightarrow CO_3^{2-} \tag{16}$$

In the second step a parallel path is possible, which would form an intermediate O^-:

$$O_2^{2-} + e^- \Leftrightarrow O^{2-} + (O^-)$$
$$(O^-) + e^- \Leftrightarrow O^{2-}$$
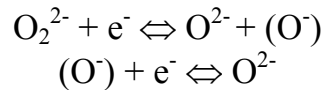
Superoxide pathway

If superoxide is the dominant reacting species, then

$$3\ O_2 + 2\ CO_3^{2-} \Leftrightarrow 4\ O^{2-} + 2\ CO_2$$
$$O^{2-} + e^- \Leftrightarrow O_2^{2-}$$

this is then followed by the steps (15) & (16) of the peroxide path. It is interesting to note the role of peroxide in the superoxide reaction path. The fact that peroxide is thermodynamically more stable than superoxide in most of the eutectics studied should favour the peroxide path. Still the peculiar role of CO_2 (e.g., rate determining step is either CO_2 dissolution or oxide-CO_2 recombination) is not known.

4.1.6. Preparation methods

Transition metal oxides are usually prepared by thermal decomposition of an appropriate mixture of metal salts or by the solid state reaction of metallic oxides. The nature of the precursor and the temperature of calcination appear to be the primary factors influencing the properties of the resulting oxides. Particle size, non-stoichiometry, and morphology of the layer are strongly influenced by the nature of the precursor. For instance, chlorides as precursors leave residual chlorine in the oxide lattice, while nitrates do not. Various distorted lattices can thus result. Moreover, the range of temperatures where decomposition takes place depends on the nature of the precursor [112].

The temperature of decomposition affects both the composition and crystallinity of the layer. Non-stoichiometry is usually higher at lower temperatures. More ordered lattices are obtained at higher temperatures. But the surface area of the resulting materials will be less and not good for electrochemical studies. In order to prepare finer and more homogeneous oxides freeze drying, spray pyrolysis, plasma spray, sputtering and precipitation followed by thermal decomposition methods are exploited. In general, poorly crystalline to amorphous layers are obtained at low temperatures which impart higher activity but lower stability to the oxide. Spray pyrolysis is also a thermal decomposition method, but the precursor solution is sprayed onto the support heated at the decomposition temperature. The deposition can be more reproducible but the impact gives more adhesion. Plasma spray and reactive sputtering have been suggested as alternatives. The latter, however, normally produces smooth stoichiometric surfaces and is thus more suited for the preparation of reference oxide samples. Most of the oxides were prepared by precipitation method. This is a simple and reliable method to obtain high surface area oxides. The preparation of the high surface area $Pb_2Ru_{1.75}Pb_{0.25}O_{7-y}$ was described by Horowitz *et al.* [100] as follows: In brief, (1:1.25) molar ratio of $RuCl_3 \cdot 3H_2O$ and $Pb(NO_3)_2$ were dissolved in aqueous solution at 348 K under constant stirring and purging of the solution with O_2 for 24 h. Approximately, 6% KOH was added to the solution so as to maintain a pH 13.5. The filtered product was washed with distilled water until any alkali present was removed. It was then annealed at 403 K for 24 h. $Ni_xCo_{3-x}O_4$ mixed valence oxides were synthesized by thermal decomposition of stoichiometric amounts of the nitrate salts $Co(NO_3)_2 \cdot 6H_2O$ and $Ni(NO_3)_2 \cdot 6H_2O$ in air at 523 K for 2 h followed by heating at 573 K for 16 h [95]. Amorphous citrate precursor method and malic acid precursor methods are also promising methods to prepare high surface area materials. For example, the catalyst, $La_{0.6}Ca_{0.4}CoO_3$ powder was prepared by an amorphous citrate precursor method in the following manner [113]. A solution containing a mixture of citric acid and constituent metal nitrates, including $La(NO_3)_3$, $Ca(NO_3)_2$, and $Co(NO_3)_2$, were gradually evaporated at 348 K until a blue paste was formed. The molar ratio of

citric acid to the metal nitrates was 1:1, and the molar ratio of metal nitrates for $La(NO_3)_3$, $Ca(NO_3)_2$, and $Co(NO_3)_2$ is 0.6:0.4:0.1. The blue paste was evaporated to dry at 363 K for 48 h until it changed into a blue solid; the solid was then pre-calcined at 473 K for 2.5 h and the calcinations was continued for 2.5 h at increasing temperatures up to 973 K to form the perovskite phase.

One of the requisites of electrocatalysts is to possess a large working surface area. Therefore, it has been proposed to follow sol-gel and microemulsion methods to prepare oxides for electrocatalysis. These methods are used to prepare catalysts with small particle size, and it has been believed that these features could be useful for electrodes. These procedures produce the metallographic precursor that decomposes at low temperatures, thus producing fine particles. Carbon powders, added in the early stages of preparation, have been reported to increase specific surface area of oxides. A typical procedure described by Raghuveer *et al.* [105] is as follows. The stoichiometric amounts of lead nitrate and ruthenium chloride trihydrate required to prepare $Pb_2Ru_{1.95}$ $Pb_{0.05}$ $O_{7-\delta}$ were dissolved in 67 ml of water. This aqueous solution was added to AOT/n-heptane mixture with vigorous stirring to prepare water in oil emulsion I. Microemulsion II was prepared by adding KOH in AOT/n-heptane under stirring. These two microemulsions were mixed together with stirring at room temperature. The reaction proceeded for 2 h. After that acetone was added to cause sedimentation of Pb-Ru hydroxides. The washed particles were dried in air oven maintained at 393 K for 2 h and ground powder was finally calcined at 773 K for 2 h in air. Same authors prepared $Pb_2Ru_{1.95}$ $Pb_{0.05}$ $O_{7-\delta}$ by sol-gel method [105] in the following manner. Stiochiometric amounts of lead nitrate and ruthenium chloride trihydrate were taken in one burette and 5% KOH in another burette. These solutions were released into the polyacrylamide gel solution maintained at 350 K with stirring. The flow rates are adjusted in such a way that pH of the solution was maintained at 7.5. After the completion of precipitation, it was aged for 30 min at 350 K, followed by filtration and drying at 373 K for 2 h. the precursor was calcined at 773 K for 2 h in air. A typical procedure described by Yuasa *et al.* [86] for the preparation of La-Sr-Mn-Fe-O perovskite oxide is as follows; Aqueous solutions of metal nitrates of the intended oxides and Me_4NOH as precipitant were separately transformed into reverse micelle dispersions by using poly(oxyethylene)5-lauryl ether surfactant and cyclohexane. These dispersions were mixed together to derive a reverse micelle dispersion containing mixed hydroxides as precursors of the oxides, into which C powder suspended in cyclohexane was added with agitation. The suspension was destabilized with EtOH and the resulting precipitate (C-supported precursors) was calcined in a N_2 atmosphere to prevent the C matrix from being combusted. Single-phase oxides supported on C were obtained by calcination at 973 K.

Recently, microwave assisted method was used to synthesize various metal oxides. Microwave synthesis has given products with good phase purity and degree of crystallinity and nanoscale particles. Also larger surface area and smaller particles, but also bigger crystallites compared to conventional methods have been obtained. Recently several spinels and other oxides have been synthesized by applying microwave irradiation. The effect of microwaves varies from material to material. If the starting materials are not good susceptors to microwaves, it is necessary to use a secondary susceptor that assists the initial heating. Amorphous carbon powder can be used for this purpose since it absorbs microwaves rapidly. A typical procedure to prepare $MnCo_2O_4$ described by Nissinen *et al.* [94] is as follows; Carbon was mixed with aqueous solutions of metal nitrates e.g., $Mn(NO_3)_2$ and $Co(NO_3)_3$ followed by heating in microwave oven at 125 W for 10 min. Various methods used to prepare the mostly investigated systems for oxygen reduction reaction and the corresponding activities are shown in Table 3.

Table 3. Preparation methods, electrocatalytic activities and selectivity towards oxygen reduction of transition metal oxides compared to Pt.

Catalyst	Preparation method	Electrolyte medium	No. of electrons transferred	Catalytic activity towards O_2 reduction vs. Pt	Reference
$Ln_2NiO_{4+\delta}$ (Ln = La,Nd,Pr)	Amorphous citrate precursor method	Alkali	n. r	n. r	114
$LaMnO_3$/carbon	Reverse homogeneous precipitation using chelating compound	Alkali	n. r	n. r	115
TiO_2	Electrodeposition	Acid/Alkali	4/2	n. r	60
$La_{1-x}Sr_xMn_{1-y}Fe_yO_{3+\delta}$ (x = 0 – 0.4, y = 0 – 0.8)	Reverse micellar method	Alkali	n. r	Excellent	86
$CoFe_2O_4$/PPy	Electrodeposition	Alkali	n. r	n. r	96
$REMn_2O_5$ (RE = Dy,Ho,Er,Tm, Yb and Lu) $Er_{0.76}Zr_{0.11}Ca_{0.13}Mn_2O_5$	Amorphous citrate precursor method	Alkali	n. r	n. r	116
$LaMnO_{3+\delta}$/carbon	Reverse micellar method	Alkali	n. r	n. r	117
$La_{0.6}Ca_{0.4}CoO_3$	Amorphous citrate precursor method	Alkali	n. r	n. r	113
$Ni_xCo_{3-x}O_4$/PPy	Thermal decomposition	Alkali	n. r	n. r	95
$La_{1-x}MnO_{3+\delta}$, $La_{1-x}M_xMnO_{3+\delta}$ thin films	Sputtering	Alkali	n. r	n. r	118
$Pb_2Ru_{1.95}Pb_{0.05}O_{7-\delta}$	Reverse micellar method, sol-gel	Acid	n. r n. r	Comparable	105
$Mn_xCo_{3-x}O_4$ (0<x<1) thin films	Spray pyrolysis	Alkali	n. r	n. r	119
$Ni_xAl_{1-x}Mn_2O_4$ (0<x<1)	Sol-gel	Alkali	n. r	n. r	120
$La_{1-x}A_xMnO_3$ (A = K,Na,Rb)	Solid state method	Alkali	n. r	n. r	121
$La_{1-x}A_xFe_{1-y}Co_yO_3$ (A = Ca, Sr, Ba) (x = 0-0.5, y = 0-0.5)	Malic acid precursor method	Alkali	4	n. r	122

Table 3. Continued

Co_3O_4, $PbCo_5O_x$	Sol-gel	Alkali	4	n. r	123
$MnCo_2O_4$	Amorphous citrate precursor method	Alkali	4	n. r	124
$La_{0.6}Sr_{0.4}Co_{1-x}Fe_xO_3$	Malic acid precursor method	Alkali	n. r	n. r	125
$Bi_2Ru_2O_7$ thin films	Sputtering	Alkali	n. r	n. r	126
$Cu_{1+x}Mn_{2-x}O_4$ (0<x<0.4) thin films	Spray pyrolysis	Alkali	n. r	n. r	127
$Cr_{0.25}Cu_{0.75}Mn_2O_4$	Ceramic method	Alkali	4	n. r	128
Mn_5O_8	Amorphous citrate precursor method	Alkali	4	n. r	129
$Pb_2Ru_{2-x}Pb_xO_{7-\delta}$, $Bi_2Ru_{2-x}Bi_xO_{7-\delta}$	Precipitation method	Acid	n. r	n. r	101
$Pb_2Ir_2O_{7-\delta}$, $PbBiRu_{2-x}O_{7-\delta}$	Precipitation method	Alkali	n. r	n. r	130
$La_{0.5}Sr_{0.5}CoO_3$, $LaCoO_3$, $SrCoO_3$	Amorphous citrate precursor method	Alkali	n. r	n. r	131
$CaMnO_{3-\delta}$	Thermal decomposition	Alkali	4	n. r	132
$Pb_2Ir_{2-x}Pb_xO_{7-\delta}$, Nd_3IrO_7	Solid state method	Alkali	n. r	n. r	133
MnO_2/carbon	Impregnation method	Alkali	n. r	n. r	134
$Ln_{0.4}Sr_{0.6}Co_{0.8}Fe_{0.2}O_{3-\delta}$ (Ln = La,Pr,Nd,Sm,Gd)	Ceramic method	YSZ	n. r	n. r	135
$(La_{0.5}Sr_{0.5})_xMnO_3$ thin films	Sputtering	YSZ	n. r	n. r	136
$(La,Sr)MnO_3$	Coprecipitation, solid state method	Alkali	n. r	n. r	137
$La_{1-x}Sr_xAl_yFe_{1-y}O_3$ (x = 0.2, y = 0.1-0.4)	Glycine-nitrate combustion synthesis method	YSZ	n. r	n. r	138
$Pb_2[Pb_{0.58}Ru_{1.42}]O_6O'_{0.5}$/carbon	Precipitation method	Alkali	n. r	Comparable	103
$Cu_{1.4}Mn_{1.6}O_4$/PPy	Thermal decomposition	Acid/Alkali	n. r	n. r	139

(n. r = not reported)

4.2. Transition metal chalcogenides

Chevrel phases based on metal clusters constitute another class of materials that show activity for oxygen reduction. Some of these materials selectively reduce oxygen to water even in the presence of methanol by the direct transfer of four electrons under acidic conditions, which makes them as promising cathode materials for electrochemical devices such as PEMFC and DMFC.

Ternary chalcogenides of the formula $M_xMo_6X_8$ (M= Cu, Ag, Ni, Fe, Pb, rare earth, etc. and X = S, Se, or Te) have been first synthesized by Chevrel *et al.* [140] in 1971 and therefore are often referred to as Chevrel compounds. Ternary phases have structures closely related to those of binary molybdenum chalcogenides Mo_6X_8 (X= S, Se and Te). The Mo_6X_8 unit is shown in Figure. 10. These are characterized by a central octahedral metal cluster in which the delocalization of electrons leads to high electronic conductivity and also these clusters act as a reservoir for electronic charge carriers while maintaining a stable electrochemical potential. These clusters have the ability to provide
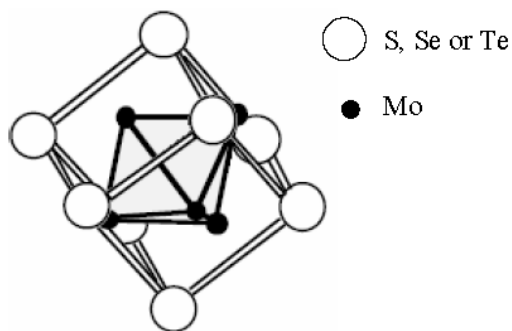
Figure 10. Illustration of the Mo_6X_8 (X = S, Se and Te) building block of the rhombohedral Chevrel phase structure [reproduced from ref. 142].

neighboring binding sites for reactants and intermediates and also have the ability to change its volume and bonding distances during electron transfer. The rhombohedral Chevrel phase consists of a stacking of Mo_6X_8 units and contains channels where additional metal atoms can be inserted, forming $M_xMo_6X_8$ compounds where M can be a variety of atoms from small to large ones (M= Ag, Sn, Ca, Sr, Pb, Ba, Ni, Co, Fe, Cr, Mn etc). Electrochemical properties of ternary Chevrel phases depend on the size and electronic configuration of the filling atoms. For example, substitution of two or four of the Mo atoms by Ru or Re gives rise to the mixed cluster compounds e.g., $Mo_4Ru_2X_8$ and $Mo_2Re_4X_8$. It leads to a contraction of the cluster which then becomes regular. According to molecular orbital calculations, the number of electrons in the intracluster bonding (Valence electron count, VEC) for Mo_6X_8 are (6x6)-(2x8) = 20 or 3.33e⁻ per molybdenum atom whereas for $Mo_4Ru_2X_8$: (4x6)+(2x8)-(2x8) = 24 or 4e⁻ per cluster atom. These electrons are essentially derived from the transition metal d-states and available at the Fermi level, E_F. By substitution of Mo atoms by suitable transition metal atoms, the position of the Fermi level will alter in such a way it suitable to the redox potential of the O_2/H_2O couple.

Electrocatalysis of the ORR on some Chevrel phases was reported for the first time in 1986 by Alonso- Vante and Tributsch [141]. They investigated the ORR activity of various Chevrel type chalcogenides and observed the increment in activity from the samples containing nonsubstituted Mo octahedra showing metallic behaviour to samples containing Ru substituted Mo octahedra ($Mo_{6-x}M_xX_8$, where X = S, Se, Te) showing semiconducting behaviour [142]. Moreover, significant changes in the overpotential for oxygen reduction was observed on metal, metal cluster and mixed metal clusters. This could be explained in terms of geometric/electronic factors through electrochemical measurements, which is supported by the density of states (DOS) at the Fermi level. Fig.11 summarizes the electrocatalytic activity of Chevrel phases in terms of the overpotential, η (at -0.01 mA/cm²) as a function
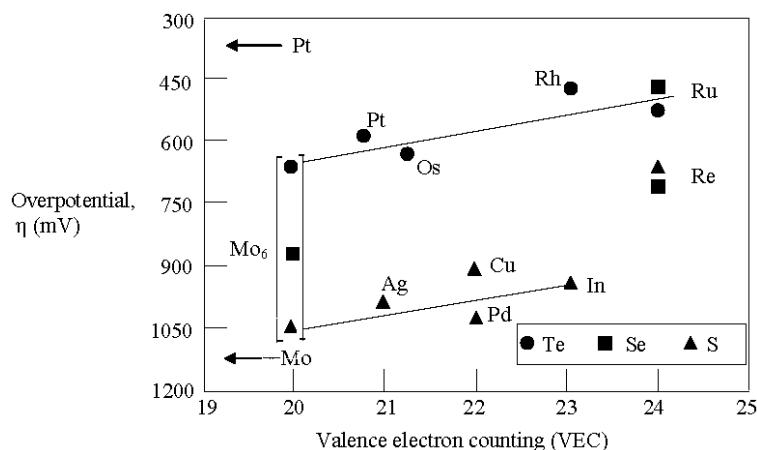
Figure 11. Dependence of the overpotential, at a current density of 10^{-2} mA/cm^2, as a function of valence electron counting (VEC) per cluster for Chevrel phases [reproduced from ref. 143].

of VEC per cluster unit. It is observed that the overpotential for ORR on the metal cluster (Mo$_6$) is decreased by 0.4 V in comparison to the metal.

When the catalytic center is enriched by electrons (3.3 to 4 e$^-$ per metal atom in the cluster) the overpotential is further decreased (0.76 V for Mo$_4$Ru$_2$Se$_8$ and 0.6 V for Mo$_4$Ru$_2$Te$_8$). On the binary series Mo$_6$X$_8$, the trend in the overpotential is as follows: Te<Se<S [144, 145]. It means that the VEC plays an important role in the ORR activity of chalcogenides. The cluster material with highest ORR activity is Mo$_4$Ru$_2$Se$_8$. This material has high DOS at the Fermi level compared to the simple metal cluster and other chalcogen contained mixed metal clusters. Its current-potential characteristics have the same shape as that of platinum electrodes. The overpotential compared to Pt is still high. The origin of this phenomenon is due to the fact that the open circuit potential becomes limited by the presence of a mixed potential (corrosion potential). The corrosion process is complex and the suggested mechanism is

$$Mo_{6-x}M_xX_8 \rightarrow Mo_{6-x}M_xX_8 + z\ Mo^{3+} + z\ e^-$$
$$z\ Mo^{3+} + y\ H_2O \rightarrow Mo_zO_y + 3z\ e^- + 2y\ H^+$$
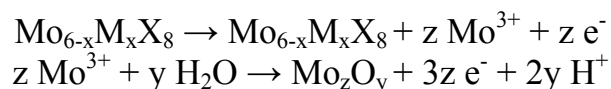
The formation of MoO$_3$ is dependent on the stabilization of metal clusters by the chalcogen atom [142]. The *in situ* EXAFS analysis [146, 147] of the Ru and Mo k-edges as a function of the electrode potential indicated that the coordination distance between Ru-Ru was sensitive in the oxygen saturated electrolyte than the co-ordination distance between Mo–Mo. The consequence of this is that it leads to a distortion of the framework due to a change in the co-ordination distance between Ru and chalcogen. It revealed that dynamics of the ruthenium centers during electrocatalysis was preferentially modified by the presence of oxygen in the electrolyte. Furthermore, there was no change in

the coordination distance between Mo and Mo (R_{Mo-Mo}) observed in the potential range of electrocatalytic current in Ar and oxygen atmospheres. However, change in the coordination distance between Ru and Ru (R_{Ru-Ru}) was evident and attained a value of ca.1 %. R_{Ru-Se} followed the same trend as that of $R_{Ru-Ru,}$ thus, assessing a certain dynamics of the cluster unit for ORR and led to the identification of the electrocatalytic center, namely the ruthenium.

Although the compounds ($Mo_{6-x}M_xX_8$) synthesized by Alonso- Vante and Tributsch [141] was thought to be related to Chevrel phases, studies by Trapp *et al*. [148] on MoRuS showed evidence for the formation of a stable RuS_x phase together with an initially unstable MoO_x phase. This composition relates to an approximate composition $Mo_2Ru_2S_5$. Based on these observations, Reeve *et al*. [149, 150] prepared a variety of compounds $Mo_xRu_yS_z$, $Mo_xOs_yS_z$, $W_xRu_yS_z$, $Rh_xRu_yS_z$ and $Re_xRu_yS_z$ supported on various surface functionalized carbon blacks and observed the best oxygen reduction activities with RhxRuySz, $Re_xRu_yS_z$ and $Mo_xRu_yS_z$. Even though the ORR activity of these materials was lower than that of platinum, their activity relative to Pt increased significantly in methanol containing electrolytes. Under the DMFC conditions, the cell utilizing $Re_xRu_yS_z$/C cathode gave working cell voltages at 100 mA/cm^2 within 100 and 80 mV of that obtained using a Pt cathode for 2 and 4 M methanol feed concentrations, respectively, where methanol permeation gave rise to appreciable degradation in Pt performance.

Later Schmidt *et al*. [151] adopted the low temperature chemical precipitation method to prepare the Mo-Ru-Se and their studies showed that a carbon-supported $Ru_xMo_ySeO_z$ had similar catalytic activity to a carbon supported Ru catalyst, suggesting only ruthenium formed the catalytic site and both Mo and Se probably did not participate in the electrocatalysis process. However, Bron *et al*. [152] demonstrated that the presence of selenium may have acted as a bridge to facilitate efficient electron transfer between the Ru-complexes and the colloids, while protecting the catalysts from the electrochemical oxidation through surface modification of the catalyst by carbonyl and carbide–carbonyl complexes or carbon compounds, which led to an enhanced stability.

The experience gained with the $Mo_xRu_ySe_z$ clusters opened the possibility to examine a family of ruthenium based chalcogenide compounds Ru_xX_y where X = S, Se, and Te. The ORR measurements performed by Solorza-Feria *et al*. [153, 154] showed higher electrocatalytic ORR activity and chemical stability than those of Chevrel phase materials. The ORR activity follows the order of $Ru_xS_y<Ru_xTe_y<Ru_xSe_y \approx Mo_xRu_ySe_z$. The geometrical parameters of Ru_xSe_y cluster like materials are similar to that of the Chevrel phase clusters. *In situ* EXAFS studies on Ru_xSe_y showed that the local structure is distorted during electrocatalytic reduction of oxygen. This is due to the interaction of molecular oxygen with the catalytic center. These observations suggest that the

intermediate surface complex during electrocatalysis is based on an oxide-like species. However, the nature of the generated surface complex species is still unknown.

Structural analysis of the active centers of Ru_xX_y (X = S, Se and Te) species by *in situ* EXAFS studies performed by Alonso- Vante *et al*. [146] suggests that the catalysts have a core of ruthenium atoms, which has triangular coordination and a direct metal-metal bond. Depending on the chalcogen, the Ru-cluster consists of two or three metal layers of different size and mutual co-ordination with chalcogen atoms coordinated to the periphery of the metal cluster. Variation of the chalcogen type affects the size of the Ru-cluster and the strength of its interaction with the chalcogen. This influences the interaction of Ru-clusters with oxygen and thus their activity in the reduction of molecular oxygen.

In order to probe active centers of Ru chalcogenide electrocatalysts during oxygen reduction, Malakhov *et al*. [147] examined the materials by *in situ* EXAFS technique. The important observations are: (1) comparison of Ru_xSe_y and Ru_xTe_y electrocatalysts shows that for the later, the Ru-O coordination numbers (CNs) are significantly higher while Ru-Ru coordination numbers are lower. Furthermore, oxygen has a stronger bond to the catalytic center in Ru_xTe_y with the bond length in the range of 2.01-2.07 Å. This is apparently due to the weaker interaction of Te with Ru in Ru_xTe_y in comparison to Ru_xSe_y. As a result, oxygen binds Ru strongly and produces RuO_x, whose catalytic activity decreases as a function of exposure of the sample to air. (2) Comparison of Ru_xSe_y and Ru_xS_y electrocatalysts shows that the coordination number (CN) of Ru to S is higher than to Se in Ru_xSe_y clusters. It means that the chalcogen S is blocking the Ru active site against molecular oxygen adsorption. This is apparently the reason for the observed lower catalytic activity of Ru_xS_y. These facts supported the experimental results of Bron *et al*. [152] who observed high current density, inhibition of formation of ruthenium oxide, negligible amount of H_2O_2 production and enhanced stability in the case of Ru_xSe_y cluster compounds. All these facts indicate that the presence of selenium alters the electronic factors of the active center and facilitates the electron transfer.

4.2.1. ORR mechanism

Since $Mo_xRu_ySe_z \approx Ru_xSe_y$ material provides a four-electron reduction pathway for the oxygen reduction, it has been studied most thoroughly in literature. The complex formation between the reduced oxygen molecule and the cluster must be the key to these systems with favourable catalytic behaviour. As a consequence of electron transfer from the transition metal cluster to the chemisorbed oxygen molecule, two distinct phenomena were to be expected.

(1) The expected upward shift of electronic levels is due to a positive charging of the cluster. Due to the semiconducting properties of the material with a Fermi level above the edge of the valence band a complete refilling of the cluster with electrons (e.g., by tunneling) is to be expected so that the metal cluster can donate electrons easily to the redox couple (O_2/H_2O) which is just below the Fermi level of the electrode [142]. This is schematically shown in Fig. 12.

(2) There is a correlation between the formal number of the valence electrons in the cluster and the metal-metal bonding distances in the cluster. Since no cooperative reaction between neighboring atoms is possible in chalcogenides due to the large interatomic distance (2.7 Å), the breaking of the –O-O- bond is facilitated and leads to the formation of water [142]. This is schematically shown in Fig. 13.
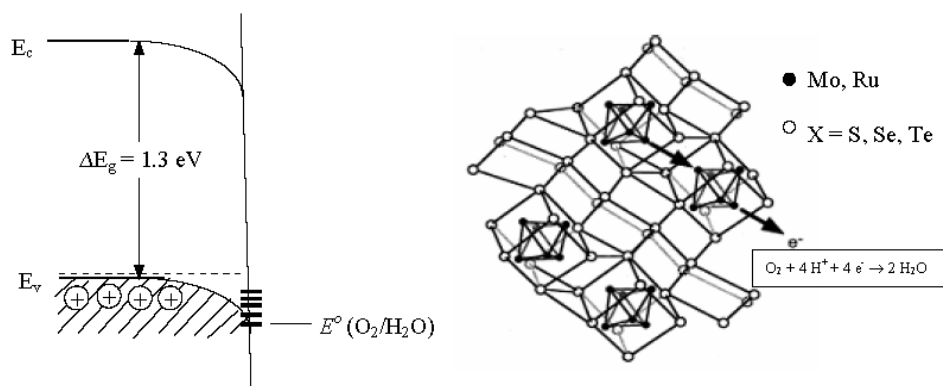
Figure 12. Schematic representation of the energy diagram and crystal structure of $Mo_xRu_ySe_z$ indicating that electron exchange occurs via the mixed metal clusters [reproduced from ref. 142, 155]
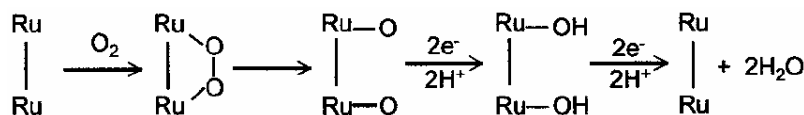
Figure 13. Schematic representation of molecular oxygen reduction on the Ru_xSe_y species [reproduced from ref. 142].

4.2.2. Preparation methods

In 1987, Alonso- Vante *et al.* [142] for the first time $Mo_4Ru_2Se_8$ synthesized via a high-temperature solid state reaction by sintering stoichiometric amounts of high purity elements in sealed quartz tubes at 1470 K for 24 h, followed by melting at 1970 K for another 48 h in a high-pressure (0.7 Gpa) argon filled furnace. After cooling, loose powder was agitated in an ampoule. In order to obtain a homogeneous product, the powder was again

thermally treated at 1970 K for 120 h. Since this process is a more complicated one and also expensive, new synthesis routes are definitely needed in order to simplify the process, reduce cost and allow the production of transition metal chalcogenides at lower temperatures in the form of nanoparticles whose size and shape can be controlled.

Trapp et al. [148] proposed a new low temperature chemical precipitation method by refluxing metal carbonyls and the corresponding chalcogen in an organic solvent such as xylene (b.p 413 K) or 1,2-dichlorobenzene (b.p 453 K) in Ar atmosphere. The obtained precipitate was filtered and washed with diethylether and then dried in air. The reaction products consist of nano-scale Ru metals and octahedral clusters of Ru, which contain carbon in the centre, surrounded by carbonyl groups. Careful examination of the $Mo_xRu_ySO_z$/$Mo_xRu_ySeO_z$ and Ru_xS_y/Ru_xSe_y systems revealed that the formed compounds had a polycrystalline and amorphous structure rather than a Chevrel phase. Mixed metal chalcogenides synthesized by this method (e.g., $Mo_xRu_ySeO_z$) showed an efficient electrocatalytic activity towards oxygen reduction in acid medium and Ruthenium/carbide/carbonyl compounds are expected to be the active center [155]. However, because this method involved some complex chemical reactions, a mixture containing several polynuclear compounds with amorphous structures could be produced, depending on the synthesis temperature. It was very difficult to separate and characterize this mixture by traditional chemical methods, due to their poor solubility, which was probably one of the drawbacks of this synthesis method. Another disadvantage of this method could be that the yield of the final product was 40–60%. Several groups such as Reeve et al. [149] and Tributsch et al. [155] carried out the same synthesis using Ru-based electrocatalysts for oxygen reduction. Reeve et al. [149] found that carbon-supported MRu_5S_5 (M =Rh or Re) could give the best electrocatalytic activity. It was even better than that of $Mo_4Ru_2Se_8$ synthesized by a high-temperature solid-state reaction. Duron et al. [156] proposed a new low temperature pyrolysis route at a synthesis temperature of 573 K. The synthesis was performed by pyrolyzing a mixture of $Ru_3(CO)_{12}$ and elemental sulphur in a sealed glass ampoule at 573 K for 24 h. The resulting powder was rinsed twice with a 1:1:1 mixture of hexane, chloroform and ethyl acetate to remove unreacted reactants. The powder was then dried overnight at 393 K. The final amorphous product, $Ru_xS_y(CO)_n$, showed considerable oxygen reduction activity. It seemed that the heating temperature played an important role in the synthesis process in order to produce a better catalyst. Tributsch et al. [155] found a reduction in catalytic activity of heated, unsupported $Mo_xRu_ySeO_z$ after release of carbon monoxide and carbon dioxide (between 523 and 623 and above 873 K). Recent work by Stephen and Campbell [157] showed that heating the carbon-supported Ru_xSe_y catalyst at 873 K completed the reaction between the ruthenium and selenium

and caused decarbonylation. Even when the heating temperature was as high as 873 K, catalyst activity was not compromised if the carbon species was present. More recently, Stephen and Campbell [157] disclosed an environment friendly aqueous method for preparing active catalysts such as Ru_xSe by eliminating the carbonyl precursors and toxic solvents like xylene. In this method, the stoichiometric amounts of active carbon, ruthenium (III) chloride and selenium dioxide were taken in a water/propanol solvent and stirred at 353 K for 1 h. The resulting mixed solution was then allowed to cool at room temperature. An aqueous solution of NaOH containing $NaBH_4$ was then added to the solution to carry out the chemical reduction reaction. The excess $NaBH_4$ was removed by heating the mixture to 353 K for 5 min. The formed powder was filtered and washed in water and dried overnight. The dried powder was then placed in a quartz lined tube furnace under nitrogen and heated to 873 K for 2 h. In this way, a carbon-supported catalyst, which has a chemical formula of Ru_xSe, was produced.

Hilgendorff *et al.*, [158] attempted to synthesize Ru_xSe_y by impregnation process. One possible drawback of this method is that the temperature used to sinter the catalyst particles is relatively high, which could reduce the catalyst active surface area. In this process, a solution of ruthenium oxalate or carbonyl complex was mixed with a carbon support to form slurry, which was then dried to remove the solvent. The formed solid was then heated to decompose the salt, in order to produce the desired form of solid carbon-Ru salt. For selenium incorporation, the solid was dispersed in a solution containing H_2SeO_3. After the chemical reaction between the carbon-Ru salt and H_2SeO_3, a Ru_xSe_y catalyst was produced. The low temperature chemical precipitation method described has the advantage of allowing the reaction performed in a solution to form bimetallic catalysts at low temperature. The prepared catalysts normally have a higher active area. However, this method was limited to those reactants with similar precipitation chemistry or property, which are easily reduced chemically to metals. In order to minimize this limitation, Tributsch *et al.* [155] followed the colloidal method described by Bonnemann *et al.* [159] in 1991. But the reproducibility was relatively low. The first step for the catalyst synthesis was to make colloidal Ru nanoparticles through $RuCl_3$ reduction in a solution of tetrahydrofuran (THF) containing $N(C_8H_{17})_4BEt_3H$, followed by addition of absolute ethanol. After that, the mixture was centrifuged (4500 rpm, 15 min) to obtain the solid powder. After the incorporation of selenium, $Ru_xSe_yO_z$ nanoparticles were prepared. The produced catalyst was tested for O_2 reduction and a fairly high electrocatalytic activity was observed. The high catalytic activity has been attributed to its large surface area, narrow particle size distribution, and abilities to prevent particle aggregation. Various methods used to prepare most of the investigated systems for oxygen reduction and the corresponding activities are given in Table 4.

Table 4. Preparation methods, electrocatalytic activities and selectivity towards oxygen reduction and methanol tolerance of transition metal chalcogenides compared to Pt.

Catalyst	Preparation method	Electrolyte medium	No. of electrons transferred	Catalytic activity towards O_2 reduction vs. Pt	Methanol tolerance vs. Pt	Reference
Chevrel phases $Mo_{6-x}Ru_xSe_8$ where x = 1.8	High temperature solid state reaction	Acid	4	Low	Excellent	142, 144
$Mo_xRu_yS_z$, $Mo_xOs_yS_z$, $W_xRu_yS_z$, $Re_xRu_yS_z$	„	Acid	n. r	Low	n. r	149, 150
Amorphous phases $Mo_xRu_ySeO_z$	Low temperature chemical precipitation method	Acid	4	Low	Excellent	148, 151, 155
Amorphous phases $Ru_xS_y(CO)_n$	Low temperature pyrolysis method	Acid	4	Low	Excellent	156
Amorphous phases Ru_xSe	Low temperature aqueous medium method	Acid	4	Comparable	Excellent	157
Amorphous phases Ru_xSe_y	Impregnation method	Acid	4	Comparable	Excellent	158
Amorphous phases $Ru_xSe_yO_z$	Colloidal method	Acid	4	Comparable	Excellent	155, 158, 159
Ru_xS_y, Ru_xTe_y	High temperature solid state reaction	Acid	4	Low	n. r	146, 147
$Ru_xCr_ySe_z$, $Ru_xFe_ySe_z$,	Low temperature chemical precipitation method	Acid	4	n. r	n. r	164, 165
$Mo_xOs_ySe_z(CO)_n$ $W_xOs_ySe_z(CO)_n$	„	Acid	4	n. r	n. r	166, 167
$M_xMo_6S_8$ (M = Ag, Ba, Cd, Zn, Sn, Pb, In, Pd)	„	Acid	<4	n. r	n. r	168
$M_xMo_{6-x}Te_8$ (M = Pt, Ru, Os, Rh)	„	Acid	<4	n. r	n. r	145

(n. r = not reported)

4.2.3. Oxygen reduction activity and stability of the catalysts

In 1989, Alonso- Vante *et al.* [144] reported sustained electrocatalytic activity of $Mo_4Ru_2Se_8$ for the oxygen reduction, without degradation, in the presence of 1-3.5 M CH_3OH. At a normal voltage range of the fuel cell operation, $Mo_4Ru_2Se_8$ was inferior to Pt catalyst by only 30–40%. Under

DMFC conditions, $Mo_4Ru_2Se_8$ as cathode and Pt/Sn as anode delivered an open circuit voltage of 0.45 V and a current density of 170 μAcm^{-2}.

Later pioneering works performed by Alonso- Vante and coworkers [146, 147, 151,160] showed the importance of ruthenium clusters towards oxygen reduction and proposed the active catalyst as Ru_xSe_y species. To test the tolerance to CH_3OH on these novel cluster materials, half-cell measurements were performed using the GDE. ORR measurements by using Ru_xSe_y/C and 30 wt% Pt/C (E-TEK) cathodes containing 1 $mgcm^{-2}$ metal loading in 2 M H_2SO_4 + 1 M CH_3OH at 313 K showed the depolarization of CH_3OH in the case of Pt/C whereas it is not in the case of Ru_xSe_y/C. at a current density of 10 μAcm^{-2} the potential is shifted by 0.14 V in negative direction whereas Ru_xSe_y/C remains selective and thus showed better performance than Pt/C at lower current densities [161, 162]. In the same experiment, Pt/C in the presence of CH_3OH reaches the same performance of Ru_xSe_y/C at 1000 μAcm^{-2}. The important feature in the iR-corrected plots is the similarity of Tafel slope (-70 mV/dec) on both the catalysts containing 14 $\mu g\ cm^{-2}$ metal. It appears that the same ORR kinetics takes place on both the catalysts.

Based on the above observations, Ru_xSe_y/C material was tested as cathode material under DMFC conditions. The GDE was prepared by applying the catalyzed carbons (mixture containing the supported chalcogenide, Ru_xSe_y/C and Nafion solution) to a diffusion layer onto carbon cloth to attain a catalyst loading of 1 $mgcm^{-2}$ of Ru_xSe_y/C (18% w/w). The anode was a PtRu/C   (E-TEK) with a loading of 1 $mgcm^{-2}$ (30% w/w). For the sake of comparison in a DMFC, a cathode Pt/C (E-TEK) with an equivalent catalyst loading was used, 1 $mgcm^{-2}$ (30% w/w*).* Membrane electrode assembly (MEA) was prepared using a membrane layer of Nafion 117. This MEA was hot pressed at 403 K over 90 s and at a pressure of 6.89 MPa. The performance of both systems is compared in a single DMFC at the temperature of 363 K. Such a performance can be improved by increasing the temperature and catalyst loadings. The important observations are the selective ORR on the chalcogenide material in the presence of methanol, as verified with half-cell measurements and the similar electrochemical behavior between Ru_xSe_y/C and Pt/C in the real DMFC mode [162, 163]. Because of the high tolerance of the chalcogenide material to methanol, this measurement proves that platinum is depolarized by the methanol crossed over the electrolyte Nafion 117 membrane. With respect to the *in situ* synthesis, the novel material is far from being optimized. Therefore, the perspectives for further improvement are open, as recently pointed out by Reeve *et al.* [149, 150]. These authors produced metal-centered catalysts ($M_xRu_yS_z$) via carbonyl compounds, using sulfur as a ligand. The high selectivity (due to the presence of ruthenium atoms) for the ORR of these catalysts allowed them to determine, in real fuel cell conditions, the steady
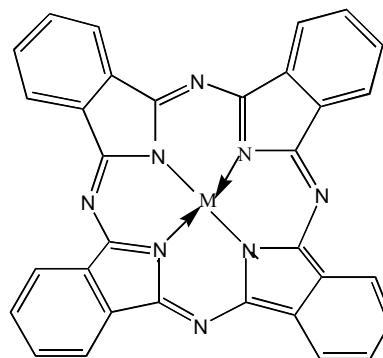
state concentration of the fuel. Recently, Stephen and Campbell [157] claimed the electrocatalytic activity of carbon-supported Ru_xSe_y catalyst prepared by the $NaBH_4$ reduction method was very close to that of carbon-supported platinum catalysts. One arrives at the conclusion that there is still a margin to optimize the distribution of the supported chalcogenide catalyst particles to obtain high current densities and also to obtain the open circuit voltage near to that at equilibrium.

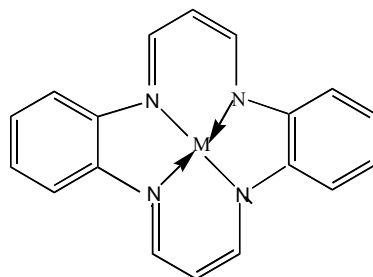## 4.3. Transition metal macrocycles

Macrocyclic derivatives of transition metals constitute a unique class of electrocatalyst for oxygen reduction. One of the characteristics of an oxygen electrode is that it chemisorbs oxygen without degradation of the catalytically active surface. Reversible adsorption has been observed in aqueous solution for some metal chelates e.g., bis(salisylal) ethylene diamine cobalt(II), heme, and Co(II) histidine. The possible application of these soluble compounds as fuel cell (for cathode) catalysts would lead to a complicated engineering system, even if the oxygen exchange kinetics was favourable. A number of insoluble metal chelates will also chemisorb oxygen; the most chemically stable of these are metal porphyrins, metal phthalocyanines and metal tetraazannulenes to some extent [169]. The reason for exploiting these materials as oxygen reduction catalysts is due to their analogous structures of enzyme catalase, which decomposes oxygen in living cells. These molecules are having square planar structures with the metal atom symmetrically surrounded by four nitrogen atoms. These nitrogen atoms are each members of ring systems, which in turn are connected by carbon atoms (porphyrins) or nitrogen atoms (phthalocyanines). A number of these are insoluble and stable in acids (8 M H_2SO_4) and bases (7 M KOH). Catalytic activity for oxygen reduction is found only with a macrocyclic ligand, which has a cyclic conjugation of 'π' electrons [31].
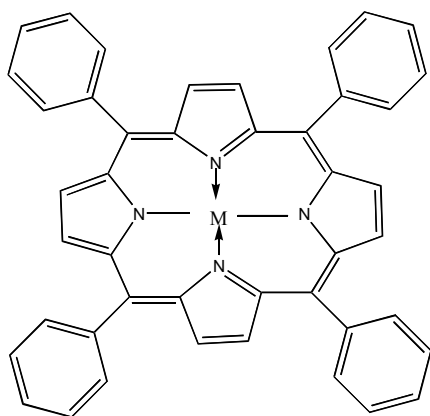
Metal tetraphenylporphyrin (M-TPP)   **Metal phthalocyanine (M-Pc)**

Metal dibenzotetraazaanulene (M-TAA)

In 1964, Jasinski [170] first reported oxygen electrocatalysis with an adsorbed transition metal macrocycle, the CoPc, adsorbed on carbon and nickel structures. Shortly thereafter, Jahnke and coworkers [171] examined polymeric metal phthalocyanines and Kozawa *et al.* [172] extensively studied the adsorbed Fe and Co phthalocyanines on pyrolytic graphite electrodes. In recent years, the desires for a low cost, catalytic oxygen electrode for fuel cells have accelerated the examination of various transition metal macrocycles as potential catalysts. Metal phthalocyanines, porphyrines, Schiff bases and related derivatives are frequently investigated. All these materials display an activity for the electroreduction of oxygen. Metal porphyrins and phthalocyanines have the advantage, in comparison to Schiff bases, that their chemical properties can be manipulated through substituents in the β- or meso-positions. Also, electrocatalytic activity and stability in acidic media appear to be enhanced for metal porphyrins and metallophthalocyanines with respect to the Schiff bases [173]. Macrocyclic M-N_4 complexes of a great variety of metals have been tested, including Fe, Co, Ru, Pd, Pt, Ir, Cr, Ni, Cu, Zn, vanadyl ion, Mo, Al, Sn, uranyl ion, Sb, Ga, Na, Ag. All experimental evidences accumulated over the years have demonstrated that macrocyclic complexes of Fe and Co appear to be the best. For some particular complexes Fe is better, for others Co is better. Oxygen reduction on most Co chelates gives hydrogen peroxide as the main product of the reaction [174, 175]. Studies conducted on substituted Co chelates have shown that even though the activity varies for each individual complex depending on the substituent, the mechanism remains the same and peroxide is always the product [174, 176]. The activity of Fe phthalocyanine is lower than that of Co phthalocyanine. The reverse is true for porphyrins. However, they suffer from low electrochemical stability, and they decompose either via hydrolysis in the electrolyte or attack of the macrocycle ring by peroxy intermediates generated during oxygen reduction [177]. Collman *et al.* [178] and Steiger *et al.* [179, 180] investigated the oxygen reduction activity of dicobalt face-to-face porphyrins, other binuclear and polynuclear Co phthalocyanines and found the direct reduction to water in acidic medium. In alkali only reduction to peroxide was observed [181]. The

motivation for this work on these compounds was to fine tune their structure to form, for example, a cage for O_2, stretching this molecule appropriately between two metal atoms in the porphyrin, thus weakening the O-O bond and increasing the rate of reduction of the molecule. Since the distance between two Co centres is 4 Å, this facilitates the bridge adsorption of O_2 and leads to the formation of water. Even though some peroxide is always formed via a parallel mechanism. Oxygen reduction on planar dicobalt chelates [182] gives water in alkaline solutions and peroxide in acid, which is exactly opposite of what is observed with face-to-face Co porphyrins. This could be explained by assuming that O_2^- is the intermediate: in acid it will be rapidly attacked by protons, forming hydrogen peroxide. In alkaline solution it is more stable, enabling bridge adsorption and leading to water formation. The difference in behaviour observed for cofacial and planar dicobalt complexes is due to the binding of oxygen molecule in a trans- and cis- manner respectively. They have also reported on the behaviour of a set of cobalt porphyrines having π-acid ligands pendant to the porphyrin ring as electrocatalysts for the reduction of O_2. Four electron reduction of O_2 to water can also be achieved by using two different metal centres, as proposed by Bettelheim *et al*. [183] and Steiger *et al*. [179] for electropolymerized layers of Co and Mn tetra(o-aminephenyl)porphyrins and multilayers of Co tetra-4-pyridyl porphyrin. Tse *et al*. [184] have found that electropolymerized Co tetraaminophthalocyanines (CoTAPc) also promotes the four electron reduction mechanism. However, it was only observed at high polarizations. At low polarization peroxide is formed on poly-CoTAPc.

Iron chelates, in contrast to Co chelates, reduce oxygen mainly to water. Zagal *et al*. [31, 174, 175] performed oxygen reduction experiments on iron tetrasulfonated phthalocyanine (FeTSPc) in alkaline solution and observed four electron reduction mechanism at low overpotentials whereas two electron reduction at high overpotentials. When FeTSPc is incorporated in polypyrrole, four elecron reduction of oxygen is increased compared to the adsorbed layers. It was suggested that peroxo dimeric FeTSPc species could exist within the polymeric film. The same authors conducted oxygen reduction on a mixture of CoTSPc and FeTSPc adsorbed on graphite in alkaline solution and observed the linear decrease of hydrogen peroxide production with increasing Fe content in the mixture. The results strongly indicated the dual mechanism on Fe centres is unlikely and suggest that the direct water formation on a single Fe site is probable. It is also possible that hydrogen peroxide is decomposed or reduced on the same site on which it is formed. Thereafter, researchers investigated the oxygen reduction activity of various Fe chelates and found that the nature of ligand is also an important in hydrogen peroxide reduction or decomposition. When comparing the activity of FeTPP-Cl [185] and FeTPyPz, the latter does not promote the reduction of peroxide. Tanaka *et al*. [186] found

the formation of water at low overpotentials whereas peroxide at high overpotentials on FeTPyPz (iron tetrapyridinoporphyrazine). A relation exists between an increasing hydrogen peroxide decomposition rate constant and increasing oxygen reduction activity in acid solution. All the experimental results show that iron porphyrin and phthalocyanine derivatives exhibited highest oxygen reduction activity with single site for O_2 adsorption. In order to increase the activity and stability, metal chelates were adsorbed on carbon and investigated the oxygen reduction measurements. It has been shown that the carbon with basic functional groups is the most effective type of support. However, the results were not satisfactory in terms of both the activity and stability of these Co and Fe chelates. Moreover activity was far less compared to the state-of-art Pt electrocatalysts.

Several research groups [187-200] have reported that the heat treatment of transition metal macrocycles adsorbed on carbon supports greatly improves their stability as electrocatalysts for oxygen reduction without substantial degradation and, in some instances, enhancing their overall catalytic activity. Usually heat treatment is carried out in argon or nitrogen atmosphere at temperatures between 673–1273 K. The maximum activity has been observed in the range of 773-1073 K for most of the chelates adsorbed on carbon support. For example, better oxygen reduction activity for heat treated FeTPP/CDX975 carbon at 873 K and for FePc/CDX975 carbon heat treated at 773 K have been observed [200]. These results are shown in Tables 5 and 6. The optimum temperature for maximum activity depends on the metal, the ligand, and nature of support. What is left on the electrode surface after the heat treatment consists largely of the metal atoms of the porphyrin. The distances between such metal atoms will correspond to the diameter of the adsorbed organic. Correspondingly, the high temperature will have bound the atom to the carbon surface. Thus, the individual atoms would be acting catalytically; they would not be able to lose catalytic power by aggregating to form clusters in which most of the atoms are hidden from reactants inside the clusters.

Although much effort has been devoted to determine the composition and the structure of the electrocatalytic center that is formed upon pyrolysis, some controversies still exist and a number of various hypotheses have been put forward to explain the increased activity and stability of the pyrolyzed material.

1. Formation of a highly active carbon with functional chemical surface groups. In this hypothesis, the transition metal atoms are not directly responsible for the increased oxygen reduction capability but instead catalyze the formation of the highly active carbon surface.
2. Chelate redispersion: enhancement of the activity was attributed initially to an improvement in chelate redispersion. But redispersion cannot explain

Table 5. Activity for Oxygen reduction of untreated and heat treated FeTPP/CDX975 catalysts [from ref. 200].

Heat treatment temp (K)	Iron content (wt %)	Nitrogen content (wt %)	Oxygen reduction activity at 0.503 V vs. Ag/AgCl, sat KCl (mA/cm^2)
Untreated	1.96	2.3	0.0
373	n. m	2.2	0.0
473	n. m	2.14	0.0
573	n. m	2.1	0.08
673	n. m	1.87	1.1
773	n. m	1.74	1.8
873	1.97	1.7	3.81
973	n. m	1.65	2.72
1073	n. m	1.3	1.6
1173	n. m	1.04	1.2
Pt	-	-	5.1

(n. m = not measured)

Table 6. Activity for Oxygen reduction of untreated and heat treated FePc/CDX975 catalysts [from ref. 200].

Heat treatment temp (K)	Iron content (wt %)	Nitrogen content (wt %)	Oxygen reduction activity at 0.503 V vs. Ag/AgCl, sat KCl (mA/cm^2)
Untreated	1.86	1.94	0.0
373	n. m	1.62	0.0
473	n. m	1.58	0.0
573	n. m	1.5	0.13
673	n. m	1.48	0.4
773	n. m	1.4	2.4
873	1.85	1.2	2.2
973	n. m	1.1	0.44
1073	n. m	0.4	0.31
1173	n. m	0.18	0.18

(n. m = not measured)

the improved stability. Therefore, it does not describe the heat treatment process. However, it is likely that improvement of the bonding of the chelate to the support during the early stages of the pyrolysis occurs, probably via sublimation and re-adsorption or that initially physisorbed species become chemisorbed.

3. Formation of a modified carbon surface on which transition metal ions are adsorbed, principally through interactions with the residual nitrogen derived from the heat-treated macrocycles i.e., retention of the metal-N_4 active site even after the pyrolysis treatment.

4. Polymerization of the metal chelate during heat treatment has also been suggested as an explanation for improvement in electrocatalytic activity. It has been suggested that polymerization only occurs when the metal macrocycle is unsupported. Lalande *et al.* [204] have found that polymerization of the complexes does occur in the presence of the carbon support, but for heat treatment temperatures lower than 673 K. However, the oxygen reduction activity lies in the order: monomer<polymer<heat treated supported catalysts.

5. Presence of metal oxides and metal particles: During the pyrolysis of metal chelates at high temperatures, some fraction of the metal particles or metal oxides can be formed. These species may have some activity in alkaline solutions, but in acid they should dissolve and leave the electrode surface.

The most widely accepted model to explain the improvement in activity and stability is the creation of M-N_4 moiety on carbon matrix or simply MN_4C_x species during the pyrolysis.
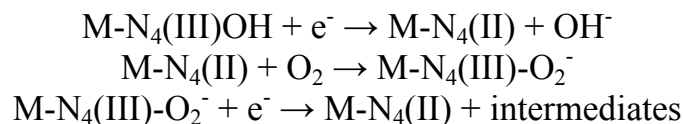
Studies on iron and cobalt macrocycles adsorbed on carbon support had shown that the reduction of oxygen is enhanced by the presence of MN_4C_x (where M= Fe and Co) species. At first Joyner *et al.* [206] proved the existence of CoN_4 with Co-N distance as ≈ 1.95 Å at medium temperatures by using EXAFS in the case of cobalt porphyrins (CoTPP, CoTBP). Later Wingerden *et al.* [207] carried out EXAFS measurements to study the effect of heat-treatment on the oxygen reduction activity by adsorbing 5,10,15,20-tetra-(p-chlorophenyl) porphyrinatocobalt on carbon. This study shows that (i) upon adsorption the Co chelate remains intact, (ii) after heating at 823 K, when the oxygen reduction activity is at its maximum, all Co is still present in its original (Co-N_4) environment and (iii) at higher temperatures the CoN_4 moiety decomposes to form, ultimately, metallic Co, with a concomitant decline in catalytic activity. XAS measurements studied by Martin Alves *et al.* [205] on CoPc/C also demonstrated the persistence of the Co-N_4 moiety upto 973 K while ToF-SIMS results also detected for the same precursor fragments containing Co bound to N upto 973 K. Yeager *et al.* [189] also detected the presence of Co-N_4 moiety on the basis of *in situ* Mossbauer

experiments using CoTPP. XRD, XPS, TEM and ToF-SIMS studies on heat-treated FeTPP/C and CoTPP/C catalysts by Faubert *et al.* [195] had shown the presence of metal-N$_4$ part in the temperature range of 773-973 K, where the ORR activity is maximum and disappearance of metal-N$_4$ moiety and presence of metal particles, metal oxides and metal carbides at higher temperatures (>1073 K). Mossbauer spectral studies [208] of unsupported FePc and CoPc heat-treated at 773-973 K also indicate that the N$_4$-M moiety is mainly retained. Lalande *et al.* [196, 204] also observed the ions containing the metal bound to nitrogen using ToF-SIMS for Co and Fe phthalocyanines pyrolyzed at temperatures upto 973 K and porphyrins pyrolyzed upto 1073 K. The same authors [204] investigated the importance of the presence of nitrogen and Fe in the generation of active sites by using two independent organic precursors, namely polyvinylferrocene as a precursor of Fe and acetonitrile as a souce of nitrogen. The results show the essentiality of the Fe-N bonds on carbon matrix to exhibit the oxygen reduction activity. The results obtained by Dodelet and co-workers [195, 196, 201-204, 217] open the door to a more versatile way to prepare catalysts. Several authors reported the generation of active sites by using independent metal, nitrogen and carbon precursors. Even though the results were satisfactory, valuable information was obtained. Choi *et al.* [209] also reported the presence of Fe-N$_4$ at medium temperatures and iron oxides and carbides at higher temperatures based on EXAFS measurements. ToF-SIMS measurements studied by Lefevre *et al.* [210-212] on FeTMPP on carbon also proved the existence of FeN$_4$ at medium temperatures (873 K) and FeN$_2$ at high temperatures (1073 K). Recently, the same authors [213] performed ToF-SIMS studies on CoTMPP adsorbed on carbon and proved the existence of CoN$_4$ moiety alone where the ORR activity is maximum but not observed the CoN$_2$ moiety at any heat treatment temperature.

4.3.1. ORR mechanism

For a qualitative explanation of the activity of these systems, different concepts were developed. Application of the MO theory [171] to these systems has shown that the highest interaction of O$_2$ with the central metal ion is obtained with Fe(II) and Co(II). The higher this interaction, the more the O-O bond is weakened and the more easily the molecule is reduced. Another approach has been given by Ulstrup [214]. If the electronic levels of the electrode and reactant lie too far apart, the transition of electrons is improbable. The catalysts should then act as a mediator supplying intermediate levels thus increasing the probability of electron transport. A third concept is that of redox catalysis developed by Beck [215]. In this concept the redox potential of the central metal ion is crucial. In this concept, the interaction of O$_2$ molecule with metal center in the macrocycle causes a

partial electron transfer from the frontier orbitals of metal to the frontier orbitals of the O_2. The precursor or adduct formed, undergoes further reduction to give intermediate species like peroxide which can be the product or decomposed/reduced further to give water. The crucial steps in the catalytic cycle are given as follows:

$$M\text{-}N_4(III)OH + e^- \rightarrow M\text{-}N_4(II) + OH^-$$
$$M\text{-}N_4(II) + O_2 \rightarrow M\text{-}N_4(III)\text{-}O_2^-$$
$$M\text{-}N_4(III)\text{-}O_2^- + e^- \rightarrow M\text{-}N_4(II) + \text{intermediates}$$

According to this redox mechanism, the redox potential of M(III)/M(II) must be located within an appropriate, rather narrow window of potential values to obtain maximum activity. When the activity for the oxygen reduction is compared with the redox potential of the M(III)/M(II) transition of different metal chelates a volcano shaped curve is obtained [51]. However, recent studies of different substituted Pc's have revealed that the lower the electron density on the metal center, the higher the catalytic activity for O_2 reduction. For studies conducted with substituted Co phthalocyanines, when the logarithm of the rate constant (taken at constant potential) of the electroreduction of O_2 is plotted versus the Co(III)/Co(II) redox potential of different substituted phthalocyanines (Co-Pcs), for graphite electrodes modified with these complexes, a straight line is obtained. Log k decreases as the driving force of the phthalocyanines increases (the driving force is represented by the Co(III)/Co(II) redox potential) so the greater the reducing power of the CoPcs, the less is the activity for O_2 reduction. This was explained in terms of the chemical intermolecular hardness of the system, i.e., the more the separation between the energy of the frontier orbitals of the donor (Co-Pc) and the acceptor (O_2), the less the reactivity. These studies reveal that questions still remain open on the role of the redox potential in determining the catalytic activity. However, most authors agree that the redox mechanism requires the stability of the 3+ and 2+ oxidation states of the metal, needed for oxygen activation in the potential region of interest for O_2 reduction. It has been found that Co and Fe porphyrins are active as long as the 3+ oxidation state is accessible at a given potential. However, for some Co complexes, O_2 reduction takes place at potentials far removed from the potential of the Co(III)/Co(II) [178]. For FeTsPc the activity decreases if the Fe(II)TsPc is reduced to Fe(I)TsPc, as the complex becomes less effective for the four electron reduction process. Most authors also agree that the Fe(II)/Fe(I) redox couple is the one that plays the crucial role in the activation of the O_2 molecule [174, 175]. This assumption was based on *in situ* electroreflectance measurements, which suggest that Fe(I)Pc interacts with oxygen but Fe(II)TsPc does not. However catalytic currents for O_2

reduction are observed at potentials that are closer to the Fe(III)/Fe(II) than do the Fe(II)/Fe(I) couple and this is true for many Fe macrocyclic complexes studied in the literature.

Collman *et al.* [178] established the mechanistic details of the oxygen reduction process on dicobalt face-to-face porphyrins by bridge mode of adsorption of O-O on two cobalt metal centres followed by cleavage to form water as the main product. Since the structure of MN_4C_x species generated by the pyrolysis of the carbon supported macrocycles was not known in literature, mechanism was not well established. Recently, the facile reduction of oxygen reduction on MN_4C_x (M = Fe and Co) species has been investigated by the authors from DFT calculations by assuming the tetrahedral geometry of MN_4 species [216]. The results show that the energy values of the orbitals and their directional wavefunctions of HOMO of FeN_4 (-7.20 eV) and CoN_4 (-7.72 eV) are matching with that of the π^* anti-bonding orbital (-8.18 eV) of oxygen molecule thus causing facile reduction of dioxygen.

4.3.2. Preparation methods

Various synthetic strategies were adopted in literature to form the active sites, MN_4C_x which are responsible for oxygen reduction. Those are

A. Heat-treatment of various substituted porphyrins and phthalocyanines of Fe and Co adsorbed on carbon supports [187-200]: This procedure involves the preparation of metal complexes such as iron tetraphenyl-porphyrin, cobalt tetraphenylporphyrin, iron phthalocyanines, cobalt phthalocyanines etc. followed by the adsorption on carbon support and heat-treatment at various temperatures ranging from 373-1273 K in Ar atm.

Step (i) General procedure for the preparation of metal complexes

Metal porphyrin

Phthalonitrile → Metal phthalocyanine
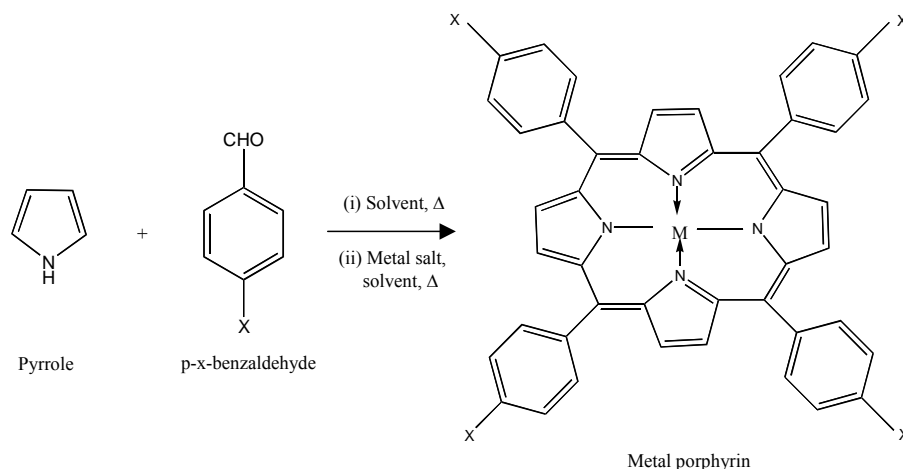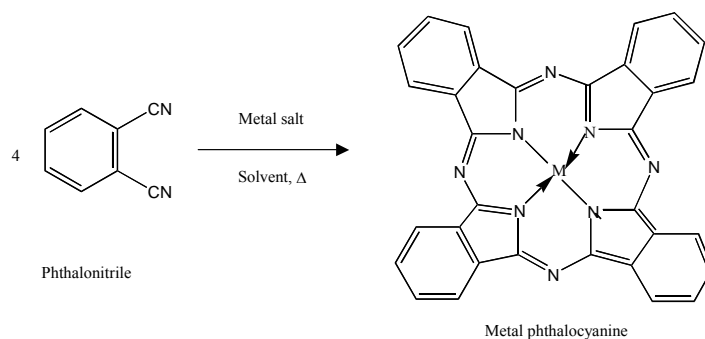
Step (ii) Adsorption of metal complex on carbon followed by heat treatment
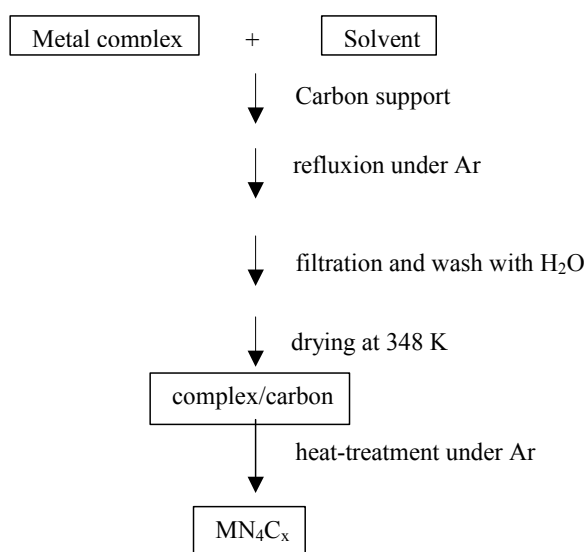
B. Pretreatment of carbon with nitrogen containing media and exploiting these materials as supports for metal salts followed by heat treatment [201-204]: This procedure involves the treatment of carbon support with nitrogen containing medium such as HNO_3 and/or NH_3, acetonitrile etc followed by adsorption of metal salt and heat-treatment.

Step (i) Modification of carbon support
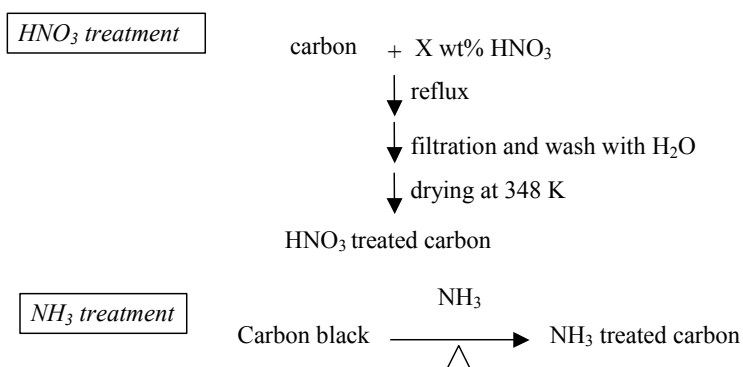
Step (ii) Addition of metal ions followed by heat treatment

Modified carbon + metal salt solution

↓ ultrasonication for 1 hr

↓ drying at 348 K

↓ heat-treatment in Ar atm

MN_4C_x
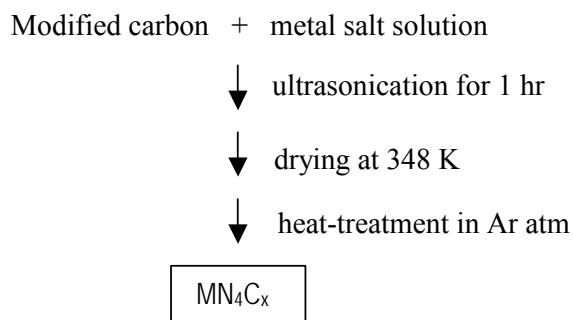
C. Heat-treatment of metal included nitrogen containing polymers, which was adsorbed on carbon [205]: This procedure involves the adsorption of solution containing polymer and metal salt to the carbon support followed by heat treatment.

Solution of polymer and metal salt
e.g., polyacrylonitrile and cobalt acetate in DMF

↓ carbon support

↓ evaporation under Ar to remove solvent

↓ heat-treatment under Ar

MN_4C_x

4.3.3. Oxygen reduction activity and stability of the catalysts

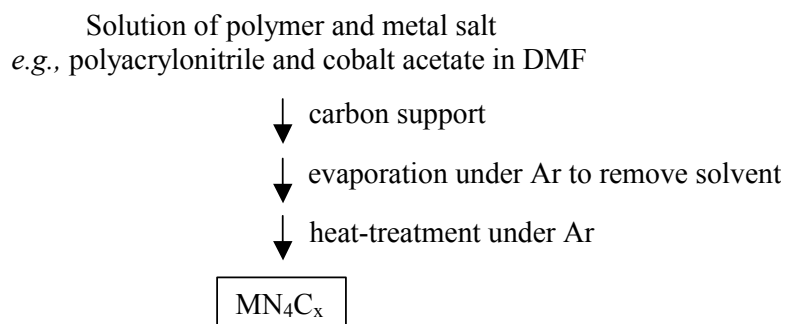The catalysts can be evaluated electrochemically in half- and full-cells. Measurements in half-cell can be obtained by the rotating disk electrode (RDE) technique while measurements in full-cell can be obtained with gas diffusion electrodes (GDE). In literature, oxygen reduction activity was measured in terms of current density at a potential where the oxygen reduction kinetics is more favorable and/or potential at which maximum reduction current occurs. But in commercial point of view, one requires a catalyst, which has the ability to reduce oxygen at higher potentials with high current densities. Among the various substituted Fe and Co macrocycles, iron and cobalt tetra methoxy-phenylporphyrins exhibited higher activity and stability. In tests in 2.5 M H_2SO_4, the catalyst prepared by heat treatment at 1073 K was stable for over 10000 hr at potentials >700 mV at a current density of 5 mA/cm^2. Most of the authors concentrated on Fe-based catalysts because of their high activity towards oxygen reduction compared to Co-based catalysts. The results obtained by fabricating the electrodes with CoTcPc/C for different temperature treatments show that the activity of the electrodes increases with

temperature up to 1173 K whereas activity was lost at 1273 K. The catalyst that is more active is comparable with that of Pt/C. Life time tests conducted on the same catalysts show the better stability up to 20 h of cell operation and also comparable with that of Pt/C [217]. Stability of the active sites generated by employing ployvinylferrocene as iron precursor and acetonitrile as a source of nitrogen exhibited the stable currents upto 300 h under fuel cell conditions. The recorded current density per mg of metal is about 1/3 of a comparable Pt containing catalyst [204]. Impressive activities for oxygen reduction was obtained using catalysts prepared via the pyrolysis of nitrogen containing polymers such as polypyrrole, polyacrylonitrile on carbon containing transition metal ions [218]. This behaviour is presumably analogous to that of the metal chelate systems. Jiang and Chu [219] have investigated methanol tolerance for the performance of the oxygen cathode for a series of heat-treated metalloporphyrins. The heat-treated CoTPP/FeTPP mixture at 873 K exhibits optimum catalytic activity for the reduction of oxygen with an onset potential of 0.9 V vs. NHE, which is comparable with that of platinum black (1.0 V vs. NHE). The catalytic activity for oxygen reduction on the heat-treated metalloporphyrin is not affected by the presence of methanol in an acidic electrolytic solution. Under similar conditions, platinum catalysts are severely affected by the presence of the same amount of methanol. No long-term life tests were reported but a loss of activity during the first 20 h of operation probably occurs as reported for other similar catalysts [217]. Convert *et al.* [220] investigated the catalytic activity of cobalt tetrazannulene (CoTAA) in half-cell conditions. The activity for the reduction of oxygen of this electrode is not affected when methanol is present in the electrolyte, whereas a noticeable decrease in activity is observed on Pt-based cathodes under the same conditions. Moreover stability of it was comparable with that of Pt-based electrodes over a period of 90 min. Gupta *et al.* [221] and Sun *et al.* [222] have studied heat-treated μ-oxo-iron(III)tetramethoxy phenyl porphyrin, iron tetramethoxy phenyl porphyrin and iron(III)octaethylporphyrin adsorbed on high surface area carbons and found high stability for oxygen reduction and insensitivity to the presence of methanol. The activity of these electrodes is not modified after periods of 24 h. the activity of these catalysts tested in a mini-fuel cell is similar to that of supported platinum (E-tek). The electrolyte was 85% H_3PO_4 equilibrated Nafion 117 membrane at 398 K and hydrated Nafion membrane at 333 K. However, supported platinum in the presence of methanol under the same conditions of the supported macrocycles showed decreased activity. RDE measurements show that the ORR activity of heat-treated (at 1073 K) FeTMPP-Cl/BP catalysts is about 1 order of magnitude lower than that of commercial platinum catalysts (20% Pt/C from E-TEK) [210]. The percentage H_2O_2 measured at their maximum catalytic activity is quite low (<5%) and comparable with that observed on commercial catalyst [212].

Number of electrons, activity and methanol tolerance found for various electrocatalysts are shown in Table 7. The negligible amount of hydrogen peroxide formed as an intermediate in these pyrolyzed catalysts reflects the stability. The characteristic features of MN_4C_x (M= Fe and Co) species like high

Table 7. Electrocatalytic activities and selectivity towards oxygen reduction and methanol tolerance of transition metal macrocycles compared to Pt.

Catalyst	Electrolyte medium	No. of electrons transferred	Catalytic activity towards O_2 reduction vs. Pt	Methanol tolerance vs. Pt	Reference
CoPc	Alakli/Acid	2	n. r	n. r	31, 174, 175
CoTSPc	Alakli/Acid	2	n. r	n. r	31, 174, 175
CoTPP	Acid	2	n. r	n. r	31
Co-Co (face-to-face porphyrins	Acid	4	n. r	n. r	178
Pillared dicobalt porphyrins	Acid	4	n. r	n. r	223
Planar dicobalt porphyrins	Alkali	4	n. r	n. r	182
Poly-CoTAPc	pH: 1.65-13	4	n. r	n. r	184
HT-CoNPc	Acid	3.8	n. r	n. r	224
Co porphyrins with $Ru(NH_3)_5$	Acid	3.5	n. r	n. r	180
FePc	Alkali	4	n. r	n. r	195, 196
FeTSPc	Alkali	4	n. r	n. r	174, 31
FeTPyPz	Alkali	4	n. r	n. r	186
HT-FeTPPCl at 873 K	Acid	4	n. r	n. r	185
FeAc/pyrrole black at 1073 K	Acid	3.9	n. r	n. r	221
FeTMPy/VulcanXC72R at 1073 K	Acid	2.7	n. r	n. r	191
FeTPPS/VulcanXC72R at 1073 K	Acid	2.7	n. r	n. r	191
FeNPc/PrintexXE2 at 773 K	Acid	3.5	n. r	n. r	224
Fe(phen)$_3$/VulcanXC72R at 1073 K	Acid	3.7	n. r	n. r	225
HT-CoTPP/FeTPP at 873 K	Acid	4	Comparable	Excellent	219
HT-FeTMPP-Cl at 1073 K	Acid	4	Comparable	Excellent	221, 210, 212
CoTAA	Acid	2	Comparable	Excellent	220
CoTcPc/VulcanXC72R at 973 K	Acid	n. r	Comparable	n. r	217
FePc/VulcanXC72R at 1173 K	Acid	4	Comparable	n. r	217

(n. r = not reported)

oxygen adsorption capacity, structural stability during oxygen adsorption and reduction, stability in acidic alkaline medium, ability to decompose H_2O_2, high electronic conductivity, methanol insensitivity and low cost make them as ideal cathode electrocatalysts for the fuel cells at low temperatures. It can be concluded that heat-treated macrocycles supported on carbon are promising for applications in low temperature fuel cells, if the decrease in activity with time of operation can be overcome.

4.4. Other electrocatalysts

Owing to the good electrical conductivity, corrosion resistance and eventual catalytic activity, metal phosphides [226], metal nitrides [227, 228], metal arsenides [229], metal tellurides [230] and metal carbides [228, 231, 232] were exploited for oxygen reduction in aqueous solutions. Mazza and Trasatti [228] investigated the oxygen reduction activity of TiN, TiC, TaC and WC in acidic solutions. They observed superior activity of WC than other investigated systems. The order of activity is, TaC<TiC<TiN<WC. Later Giner and Swette [227] evaluated the oxygen reduction activity of TiC and TiN in alkaline solutions and observed higher activity of TiN than TiC followed by Ti. Even though WC exhibited good catalytic activity, it is far less compared to the Pt catalysts and also not stable for long time. Recently, Lee *et al.* [233] examined the Ta-added WC in acid electrolyte and observed the reduction current of the WC+Ta catalyst for the ORR at a potential of 0.8 V vs. dynamic hydrogen electrode higher than that of WC (0.35 V). The enhanced electrocatalytic activity for the ORR might be caused by the presence of W carbide, which exists on the surface and/or sub-surface. The stability of the WC was significantly increased by the addition of Ta compared to the pure WC. The enhanced stability might be due to the formation of the W-Ta alloy in the WC + Ta catalyst. Apart from these materials, $Ni_{33}Ta_{41}C_{26}$, $Co_{22}TaC_{29}$, n-InP, p-InP, n-CdTe, p-CdTe, n-GaAs and p-GaAs were also exploited for oxygen reduction. But none of them showed significant activity.

5. Concluding remarks

In the past 10 years, there have been major advances in the oxygen reduction technology associated with non-noble metal based cathode electrocatalysts for electrochemical devices. A wide variety of perovskite oxides for devices at both low and high temperature operation and metal macrocyclic complexes and metal clusters for low temperature operated devices were investigated for oxygen reduction. Limited success in the development of electrocatalysts for oxygen reduction is due to the lack of understanding of the interfacial electrochemistry at three phase region (gas-liquid-solid). The information obtained from two phase region cannot be

applied to three phase region. And also the structure of the active sites responsible for oxygen reduction is not well known. As per the information available in literature, there is a still margin to improve both activity and stability of non-noble metal based electrocatalysts. These may be linked to the methods of preparation of materials in nanosize range which may exhibit higher electroactive surface area. Also new geometries of the electrodes have to be evolved to increase the active area. The search will continue till one gets a suitable alternative to platinum based materials and one can hope that some exciting and promising developments may occur in the near future.

Acknowledgement

6. References

1. W. Vielstitch, Fuel cells, Wiley/Interscience, London, 1965
2. K. Kordesch and G. Simader, Fuel cells and their applications, VCH, Weinheim, Germany 1996
3. E. Deiss, F. Holzer, O. Haas, *Electrochim. Acta* 47 (2002) 3995
4. J. P. Hoare, The Electrochemistry of Oxygen, Wiley, New York, 1968
5. F. Hine, Electrode Process and Electrochemical Engineering, Vol. 306, Plenum Press, New York, 1985
6. Martin Winter and Rolph J. Brodd, *Chem. Rev.* 104 (2004) 4245
7. http://www.eere.energy.gov/industry/imf/pdfs/lanl_chlor_alkali.pdf
8. J. O'M. Bockries and A. K. N. Reddy, Modern Electrochemistry, Vol. 2, Chapter 13, Plenum Press, New York, 1970
9. J. B. Goodenough and B. L. Cushing 'Oxide-based ORR catalysts', in "Hand book of Fuel Cells – Fundamentals, Technology and applications, Vol. 2: Electrocatalysis", Chapter 35, Wolf Vielstich, Hubert A. Gasteiger, Anold Lamm. (Eds), John Wiley & Sons, 2003
10. A. J. Appleby, *J. Electroanal. Chem.* 357 (1993) 117
11. Mario Maja, Claudio Orecchia, Morela Strano, Paolo Tosco and Marco Vanni, *Electrochim. Acta* 46 (2000) 423
12. D. B. Zhou and H. Vander Poorten, *Electrochim. Acta* 40 (1995) 1819
13. K. Kinoshita, 'Electrochemical Oxygen Technology', John Wiley & Sons, New York, 1992
14. H. Taube, *J. Gen. Phys.* 49 (1965) 29
15. J. S. Valentine, *Chem. Rev.* 73 (1973) 235
16. J. S. Griffith, *Proc. R. Sot. London Ser. A* 235 (1956) 23
17. L. Pauling, *Nature* 203 (1964) 182
18. K. Tatsumi and R. Hoffman, *J. Am. Chem. Soc.* 103 (1981) 3328
19. E. Yeager, *J. Electrochem. Soc.* 128 (1981) 160 C

20. J. P. Collman, M. Marrocco, P. Denisevich, C. Koval and F. C. Anson, *J. Electroanal. Chem.* 101 (1979) 717

21. E. W. Abel, J. M. Pratt and R. Whelan, *J. Chem. Soc. Chem. Commun.* (1971) 449

22. T. D. Smith and J. R. Pilbrow, *Coord. Chem. Rev.* 39 (1981) 295

23. L. Vaska, *Acc. Chem. Res.* 9 (1976) 175

24. A. Damjanovic, 'Mechanistic analysis of Oxygen Electrode Reactions', in "Modern aspects of electrochemistry No. 5", B. E. Conway and J. O'M. Bockries (Eds), Plenum Press, New York, 1969

25. M. R. Tarasevich, A. Sadkowski, and E. Yeager, 'Oxygen electrochemistry' in "Comprehensive Treatise of Electrochemistry", B. E. Conway, J. O'M. Bockries, E. Yeager, S. U. M. Khan and R. E. White (Eds), Plenum Press, New York, 1983

26. A. Damjanovic, 'Progress in the studies of oxygen reduction during the last thirty years', in "Electrochemistry in Transition", O. J. Murphy, S. Srinivasan and B. E. Conway (Eds), Plenum Press, New York, 1992

27. R. Adzic, 'Recent advances in the kinetics of oxygen reduction', in "Electrocatalysis", J. Lipkowski and P. N. Ross (Eds), Wiley- VCH, New York, 1998

28. A. Damjanovic, M. A. Gensaw and J. O'M. Bockries, *J. Chem. Phys.* 45 (1966) 4057

29. H. S. Wroblowa, Y. C. Pan and G. Razumney, *J. Electroanal. Chem.* 69 (1976) 195

30. N. A. Anastasijevic, V. Vesovic and R. R. Adzic, *J. Electroanal. Chem.* 229 (1987) 305

31. J. Zagal, *Coord. Chem. Rev.* 119 (1992) 89

32. Geins, R. Faure and R. Durand, *Electrochim. Acta.* 44 (1998) 1317

33. S. Mukherjee, S. Srinivasan, M. P. Sorioga and J. McBreen, *J. Electrochem. Soc.* 142 (1995) 1409

34. T. Toda, H. Igarashi, H. Uchida and M. Watanabe, *J. Electrochem. Soc.* 145 (1998) 4185

35. S. I. Pyun and S. B. Lee, *J. Power Sources* 77 (1999) 170

36. J. Perez, H. M. Vllullas and E. R. Gonzalez, *J. Electroanal. Chem.* 435 (1997) 179

37. N. M. Markovic, H. A. Gasteiger and P. N. Ross, *J. Electrochem. Soc.* 144 (1997) 1591

38. A. Damjanovic, *J. Electrochem. Soc.* 138 (1991) 2315

39. F. King, M. J. Quinn and C. D. *J. Electroanal. Chem.* 385 (1995) 45

40. Charles C. Liang and Andre L. Juliard, *J. Electroanal. Chem.* 9 (1965) 390

41. P. Gouerec, M. Savy and J. Riga, *Electrochim. Acta* 43 (1998) 743

42. S. Gupta, D. Tryk, S. K. Zecevic, W. Aldred, D. Guo, R. F. Savinell, *J. Appl. Electrochem.* 28 (1998) 673

43. T. J. Schmidt, U. A. Paulaus, H. A. Gasteiger and R. J. Behm, *J. Electroanal. Chem.* 506 (2001) 41

44. J. M. Moore, P. L. Adcock, J. B. Lakeman and G. O. Mepsted, *J. Power sources* 85 (2000) 254

45. S. Sakamoto, M. Karakane, H. Maeda, Y. Miyake and T. Susai, in '2000 Fuel Cell Seminar Abstracts: Fuel cells-Powering the 21st century', Fuel Cell Seminar, Portland, OR, 2000

46. J. B. J. Veldhuis, F. A. deBruijn and R. K. A. M. Mallant, in '1998 Fuel Cell Seminar Abstracts: Fuel cells-Clean Energy for Today's World', 1998 Fuel Cell Seminar, Palm Springs, CA, 1998

47. L. Pino, V. Recupero, M. Lagana and M. Minutoli, in '1998 Fuel Cell Seminar Abstracts: Fuel cells-Clean Energy for Today's World', 1998 Fuel Cell Seminar, Palm Springs, CA, 1998

48. K. Sawai and N. Suzuki, *J. Electrochem. Soc.* 151 (2004) A682

49. M. Bron, J. Radnik, M. Fieber-Erdmann, P. Bogdanoff and S. Fiechter, *J. Electroanal. Chem.* 535 (2002) 113

50. T. R. Ralph and M. P. Hogarth, *Platinum Met. Rev.* 46 (2002) 3

51. S. Trasatti, *Electrodes of Conductive Matallic oxides part A, B*; Elsevier Scientific Publishing Co., Amsterdam, 1980, 1981

52. C-C Chang and T-C Wen. *J. Appl. Electrochem.* 27 (1997) 355

53. C-C Chang, T-C Wen, and H-J Tien, *Electrochim. Acta* 42 (1997) 557

54. C-C Chang and T-C Wen, *J. Electrochem. Soc.* 143 (1996) 1485

55. E. R. Vago and E. J. Calvo, *J. Electroanal. Chem.* 388 (1995) 161

56. E. R. Vago and E. J. Calvo, *J. Chem. Soc. Faraday Trans.* 91 (1995) 2323

57. V. B. Baez, J. E. Graves and D. Pletcher, *J. Electroanal. Chem.* 340 (1992) 273

58. H. Kohler and W. Gopel, *J. Elctrochem Soc.* 139 (1992) 2025

59. R. Manoharan and J. B. Goodenough, *Electrochim. Acta* 40 (1995) 303

60. Slavko V. Mentus, *Electrochim. Acta* 50 (2004) 27

61. Y. L Cao, H. X. Yang, X. P. Ai and L. F. Xiao, *J. Electroanal. Chem.* 557 (2003) 127

62. L. Mao, T. Sotomura, K. Nakatsu, N. Koshiba, D. Zhang, T. Ohsaka, *J. Electrochem. Soc.* 149 (2002) A504

63. T. El Moustafid, H. Cachet, B. Tribollet and D. Festy, *Electrochim. Acta* 47 (2002) 1209

64. Chia-Chin Chang and Ten-Chin. Wen, *J. Electrochem.l Soc.* 143 (1996) 1485

65. E. R. Vago, E. J. Calvo and M. Stratmann, *Electrochim. Acta* 39 (1994) 1655

66. K. Matsuki and H. Kamada, *Electrochim. Acta* 31 (1986) 13

67. J. Yang and Jun John. Xu, *Electrochem. Comm.* 5 (2003) 306

68. J. R. Selman, in "Assessment of Research Needs for Advanced Fuel Cells" by The DOE Advanced Fuel Cell Working Group (AFCWG), S.S. Penner (Ed.), Permagon Press, New York, 1984.

69. J. D. Doyon, T. Gilbert, G. Davies and L. Paetsch, *J. Electrochem. Soc.* 134 (1987) 3035

70. J. L. Smith, G. H. Kucera and A. P. Brown, 'Development of Cathode Materials and Structures for the Molten Carbonate Fuel Cells' in "Molten Carbonate Fuel Cells Technology", J. R. Selman, D. A. Shores, H. C. Maru and I. Uchida, (Eds), Electrochemical Society, Pennington, NJ, PV90-16 (1990)

71. J. B. J. Veldhuis, F. C. Eckes and L. Plomp, *J. Electrochem. Soc. 139 (1992) L6*

72. R. C. Makkus, K. Hemmes and J. H. W. de Wit, *J. Electrochem. Soc.* 141 (1994) 3429

73. S. T. Kuk, Y. S. Song and K. Kim, *J. Power Sources* 83 (1999) 50

74. J. Soler, T. Gonza´lez, M. J. Escudero, T. Rodrigo and L. Daza, *J. Power Sources* 106 (2002) 189

75. B. Fang, C. Zhou, X. Liu and S. Duan, *J. Appl. Electrochem.* 31 (2001) 201
76. F. Li, H. Y. Chen, Ch. M. Wang, and K. A. Hu, *J. Electroanal. Chem.* 531 (2002) 53
77. C. Belhomme, E. Goyrba, M. Cassir and C. Tessier, *J. Electroanal. Chem.* 503 (2001) 69
78. H. J. Choi, S. K. Ihm, T. H. Lim and S. A. Hong, *J. Power Sources* 61 (1996) 239
79. S. Mitsushima, K. Matsuzawa, N. Kamiya and K. I. Ota, *Electrochim. Acta* 47 (2002) 3823
80. J. B. Goodenough, *J. Appl. Phys.* 37 (1966) 1415
81. Y. Matsumoto, H. Yoneyama, and H. J. Tamura, *Electroanal. Chem.* 83 (1977), 237
82. S. Muller, K. Stiebel and O. Haas, *Electrochim. Acta* 39 (1994) 1661
83. T. Hyodo, M. Hayashi, N. Miura and N. Yamazoe, *J. Electrochem. Soc.* 143 (1996) L266
84. R. Karthik, T. Mahadevan, J. Sreekanth and R. Pattabiraman, Proceedings of the International Symposium on New Materials for Fuel Cell Systems, 1st, Montreal, July 9-13, 1995.
85. Miura, Norio; Shimizu, Youichi; Yamazoe, Noboru. Nippon Kagaku Kaishi 6(1986) 751
86. M. Yuasa, G. Sakai, K. Shimanoe, Y. Teraoka and N. Yamazoe, *J Electrochem. Soc.* 151 (2004) A1690
87. E. Ivers-Tiffee, A. Weber and H. Schichein 'O$_2$-reduction at high temperatures', in "Hand book of Fuel Cells – Fundamentals, Technology and applications, Vol. 2: Electrocatalysis", Chapter 40, Wolf Vielstich, Hubert A. Gasteiger, Anold Lamm. (Eds), John Wiley & Sons, 2003
88. E. Ivers-Tiffee, A. Weber and D. Herbstritt, *J. Eur. Ceram. Soc.* 21 (2001) 1805
89. E. Ivers-Tiffee, M. Schiebl, H. J. Oel and W. Wersing, in 'Proceedings of the 13th International Symposium on Materials Science', F. W. Poulsen (Ed), Risoe, 1993
90. http://www.tf.uni-kiel.de/matwis/amat/def_en/kap_2/basics/b2_1_6.html
91. U. Morales, A. Campero and O. Solorza-Feria, *J. New Materials for Electrochemical Systems* 2 (1999) 89
92. C. C. Hays, R. Manoharan and J. B. Goodenough, *J. Power Sources* 45 (1993) 291
93. T. Kishi, S. Takahashi and T. Nagai, *Surface and Coatings Technology* 27 (1986) 351
94. T. Nissinen, T. Valo, M. Gasik, J. Rantanen and M. Lampinen, J. Power sources 106 (2002) 109
95. H. Nguyen-Cong, V. de la Garza Guadarrama, J. L. Gautier and P. Chartier, *Electrochim. Acta* 48 (2003) 2389
96. R. N. Singh, B. Lal and M. Malviya, *Electrochim. Acta* 49 (2004) 4605
97. W. J. King and A. C. C. Tseung, *Electrochim. Acta* 19 (1974) 493
98. A. C. C. Tseung and K. L. K. Yeung, *J. Electrochem. Soc.* 125 (1978) 1003
99. M. A. Subramanian, G. Aravamudan and G. V. Subba Rao, *Prog. Solid State Chem.* 15 (1983) 55
100. H. S. Horowitz, J. M. Longo and H. H. Horowitz, *J. Electrochem. Soc.* 130 (1983) 1851
101. J. M. Zen, R. Manoharan and J. B. Goodenough, *J. Appl. Electrochem.* 22 (1992) 140

102. J. M. Zen and C. B. Wang, *J. Electrochem. Soc.* 141 (1994) L51-L52
103. H. S. Horowitz, J. M. Longo, H. H. Horowitz and J. T. Lewandowski, *ACS Symp. Ser.* 279 (1985) 143
104. R. Manoharan, M. Paranthaman and J. B. Goodenough, *Eur. J. Solid State Inorg. Chem.* 26 (1989) 155
105. V. Raghuveer, Keshav Kumar and B. Viswanathan*, Indian. J. Eng. Mater. Sci.* 9 (2002) 137
106. J. B. Goodenough, R. Manoharan and M. Paranthaman, *J. Am. Chem. Soc.* 112 (1990) 2076
107. M. R Tarasevich, *Electrokhimiya* 17 (1981) 1208
108. A M Trunov, *Electrokhimiya* 22, 1986, 1093
109. A. J. Appleby and S. B. Nicholson, *J. Electroanal. Chem.* 53 (1974) 105
110. A. J. Appleby and S. B. Nicholson, *J. Electroanal. Chem.* 83 (1977) 309
111. A. J. Appleby and S. B. Nicholson, *J. Electroanal. Chem.* 112 (1980) 71
112. S. Adrizzone, M. Falciola and S. Trasatti, *J. Electrochem. Soc.* 36 (1989)1545
113. Xianyou Wang, P. J. Sebastian, Mascha A. Smit, Hongping Yang and S. A. Gamboa, *J. Power Sources,* 124 (2003) 278
114. F. Mauvy, C. Lalanne, J. M. Bassat, J. C.Grenier, H. Zhao, P. Dordor and , Ph. Stevens, *J. European Ceram. Soc.* 25 (2005) 2669
115. S. Imaizumi, K. Shimanoe, Y. Teraoka and N. Yamazoe, *Electrochem. Solid-State Lett.* 8 (2005) A270
116. Neng Li, Xiang Xu, Dan Luo, Yishi Wu, Shijie Li and Bingxiog Lin, *J. Power Sources* 126 (2004) 229
117. Masahiko Hayashi, Hiromi Uemura, Kengo Shimanoe, Norio Miura and Noboru Yamazoe, *J. Electrochem. Soc.* 151 (2004) A158
118. Keikichi Nakamura and Keiichi Ogawa, *J. Appl. Phys.* 92 (2002) 6684
119. A. Restovic, E. Rios, S. Barbato, J. Ortiz and J. L. Gautier, *J. Electroanal. Chem.* 522 (2002) 141
120. J. Ponce, J. L.Rehspringer, G. Poillerat, and J. L. Gautier, *Electrochim. Acta* 46 (2001) 3373
121. Masahiko Hayashi, Takeo Hyodo, Norio Miura and Noboru Yamazoe, *Electrochemistry (Tokyo)* 68 (2000) 112
122. Jun Gu, Sui Sheng, Guang-Qiang Li and Zhi-Tong Sui, *Wuji Cailiao Xuebao* 14 (1999) 618
123. U. Morales, A. Campero, O. Solorza-Feria, *J. New Materials for Electrochemical Systems* 2 (1999) 89
124. M. Sugawara, M. Ohno and K. Matsuki, *J. Mater. Chem.* 7 (1997) 833
125. Hyeung-Dae Moon, Ho-In Lee, *Kongop Hwahak* 7 (1996) 543
126. N.M. Markovic, P.N. Ross, *J. Electrochem. Soc.* 141 (1994) 2590
127. A. Restovic, G. Poillerat, P. Chartier and J. L. Gautier, *Electrochim. Acta* 40 (1995) 2669
128. A. F.Restovic and J. L.Gautier, J. Brazilian Chem. Soc. 5(1994) 223
129. M. Sugawara, M. Ohno, T. Endo, and K. Matsuki, *Denki Kagaku oyobi Kogyo Butsuri Kagaku* 60 (1992) 812
130. A. K.Shukla, A. M.Kannan, M. S. Hegde and J. Gopalakrishnan, *J. Power Sources* 35 (1991) 163

131. Peifang Luo, Chiyuan Wu, Yunhong Chou and Chuansin Cha, *Wuhan Daxue Xuebao Ziran Kexueban,* 3 (1986) 55

132. K. Matsuki, K. Mori and H. Kamada, *Denki Kagaku oyobi Kogyo Butsuri Kagaku* 52 (1984) 174

133. M. V. ten Kortenaar, J. F. Vente, D. J. W. Ijdo, S. Müller and R. Kötz, *J. Power Sources,* 56 (1995) 51

134. Zidong Wei, Wenzhang Huang, Shengtao Zhang and Jun Tan, *J. Power Sources,* 91 (2000) 83

135. H. Y. Tu, Y. Takeda, N. Imanishi and O. Yamamoto, *Solid State Ionics* 117 (1999) 277

136. B. Gharbage, T. Pagnier and A. Hammou, *Solid State Ionics* 72 (1994) 248

137. J. Van herle, A. J. McEvoy and K. Ravindranathan Thampi, *Electrochim. Acta 39* (1994) 1675

138. Gregory W. Coffey, John Hardy, Larry R. Pedersen, Peter C. Rieke, Edwin C. Thomsen and Mark. Walpole, *Solid State Ionics* 158 (2003) 1

139. H. Nguyen Cong, K. El Abbassi and P. Chartier, *J. Electrochem. Soc.* 149 (2002) A525

140. R. Chevrel, M. Sergent and J. Pringent*, J. Solid State Chem.* 3 (1971) 515

141. N. Alonso- Vante and H. Tributsch, *Nature* 323 (1986) 431

142. N. Alonso- Vante, W. Jaegermann, H. Tributsch, W.Honle and K. Yvon, *J. Am. Chem. Soc.* 109 (1987) 3251

143. N. Alonso- Vante 'Chevrel phases and chalcogenides', in Hand book of Fuel Cells – Fundamentals, Technology and applications, Vol. 2: Electrocatalysis, Chapter 35, Wolf Vielstich, Hubert A. Gasteiger, Anold Lamm. (Eds), John Wiley & Sons, 2003

144. N. Alonso- Vante, B. Schubert and H. Tributsch, *Mater. Chem. Phys.* 22(1989) 28l

145. C. Fischer, N. Alonso- Vante, S. Fiechter and H. Tributsch, *J. Appl. Electrochem.* 24 (1995) 1004

146. N. Alonso- Vante, I. V. Malakhov, S. G. Nikitenko, E. R. Savinova and D. I. Kochubey, *Electrochim. Acta* 47 (2002) 3807

147. I. V. Malakhov, S. G. Nikitenko, E. R. Savinova, D. I. Kochubey and N. Alonso- Vante, *J. Phys. Chem. B* 106 (2002)1670

148. V. Trapp, P. A. Christensen, A. Hamnett, *J. Chem.Soc. Faraday Trans.* 92 (1996) 4311

149. R. W. Reeve, P. A. Christensen, A. Hamnett, S. A.Haydock and S. C. Roy, *J. Electrochem. Soc.* 145 (1998) 3463

150. R. W. Reeve, P. A. Christensen, A. J. Dickinson, A. Hamnett and K. Scott, *Electrochim. Acta* 45 (2000) 4237

151. T. J. Schmidt, U. A. Paulus, H. A. Gasteiger, N. Alonso- Vante and R. J. Behm, *J. Electrochem. Soc.* 147 (2000) 2620

152. M. Bron, P. Bogdanoff, S. Fiechter, I. Dorbandt, M. Hilgendorff, H. Schulenburg and H. Tributsch, *J. Electroanal. Chem.* 500 (2001) 510

153. O. Solorza-Feria, K. Ellmer, M. Gierstig and N. Alonso- Vante, *Electrochim. Acta* 39 (1994) 1647

154. O. Solorza-Feria, S. Ramirez-Raya, R. Rivera-Noriega, E. Ordonez-Regil and S.M. Fernandez-Valverde, *Thin Solid Films* 311 (1997) 164

155. H. Tributsch, M. Bron, M. Hilgendorff, H. Schlunberg, I. Dorbandt, V. Eyert, P. Bogdanoff and S. Fiechter, *J. Appl. Electrochem.* 31 (2001) 739

156. S. Duron, R. Rivera-Noriega, M.A. Leyva, P. Nkeng, G. Poillerat and O. Solorza-Feriz, *J. Solid State Electrochem.* 4 (2000) 70

157. A. Stephen and Campbell, US Patent US2004/0096728A1 (2004).

158. M. Hilgendorff, P. Bogdanoff, M. Bron, Proceedings of the Fuel cell systems of the world renewable energy congress VII, vol. 26, 2003.

159. H. Bonnemann, W. Brijoux, R. Brinkmann, E. Dinjus, R. Fretzen, T. JouBen and B. Korall, *Angew. Chem.* 103 (1991) 1344

160. N. Alonso- Vante, P. Bogdanoff, H. Tributsch, *J. Catal.* 190 (2000) 240

161. A. K. Shukla, C. L. Jackson, K. Scott and G. Murgia, *J. Power Sources* 47 (2002) 19

162. A. K. Shukla and R. K. Raman, *Annu. Rev. Mater. Res.* 33 (2003) 155

163. K. Scott, A. K. Shukla, C. L. Jackson and W. R. A. Meuleman, *J. Power Sources,* 126 (2004) 67

164. R. Gonzalez-Cruz, O. Solorza-Feria, *J. Solid State Electrochem.* 7 (2003) 289

165. K. Su´arez-Alc´antara, A. Rodr´ıguez-Castellanos, R. Dante, and O. Solorza-Feria, *J. Power Sources* (2005) (in press)

166. 166. O. Solorza-Feria, S. Citalan-Cigarroa, R. Rivera-Noriega, S. M. Fernandez-Valverde, *Electrochem. Commun.* 1 (1999) 585-589.

167. R. H. Castellanos, A. Camperos, O. Solorza-Feria, *Int. J. Hydrogen Energy* 23 (1998) 1037

168. B. Schubert, E. gocke, R. Schoellhorn and H. Tributsch, *Electrochim. Acta* 41 (1996)1471

169. P. Vasudevan, N. Santosh, N. Mann and S. Tyagi, *Transition Met. Chem.* 15 (1990) 81

170. R. Jasinski, *Nature* 201 (1964) 1212

171. H. Jahnke, M. Schonborn and G. Zimmermann, *Top. Curr. Chem.* 61 (1976) 133

172. A. Kozawa, V. E. Zilinois and R. J. Brodd, *J. Electrochem. Soc.* 117 (1970) 1470

173. M. R. Tarasevich and K. A. Radyushkina, *Usp. Khim.* 49 (1980) 1498

174. J. Zagal, M. Paez, A. A. Tanaka, J. R. dos Santos and C. A. Linkous, *J. Electroanal. Chem.* 339 (1992) 13

175. J. Zagal, P. Bindra and E. Yeager, *J. Electrochem. Soc.* 127 (1980) 1506

176. A. Elzing, A. van der Putten, W. Visscher and E. Barendrecht, *J. Electroanal. Chem.* 233 (1987) 99

177. J. A. R. van Veen and H. A. Colijn, *Ber. Bunsenges. Phys. Chem.* 85 (1981) 700

178. J. P. Collman, P. Denisevich, Y. Konai, M. Maraocco, C. Koval and F. C. Anson, *J. Am. Chem. Soc.* 102 (1980) 6027

179. B. Steiger, C. Chi and F. C. Anson, *Inorg. Chem.* 32 (1993) 2107

180. B. Steiger and F. C. Anson, *Inorg. Chem.* 33 (1994) 5767

181. R. R. Durand, C. S. Bencosme, J. P. Collman and F. C. Anson, *J. Am. Chem. Soc.* 105 (1983) 2710

182. A. van der Putten, A. Elzing, W. Visscher E. Barendrecht and R. D. Harcourt, *J. Mol. Struct. (Theochem)* 180 (1988) 309

183. A. Bettelheim, D. Ozer, R. Harth and R. Ydgar, *J. Electroanal. Chem.* 281 (1990) 147

184. Y. Tse, P. Janda, H. Lam, J. Zhang, W. J. Pietro and A. B. P. Lever, *J. Porph. Phthal.* 1 (1997) 1

185. A. L. Bouwkamp-Wijnoltz, W. Visscher and J. A. R. van Veen, *Electrochim. Acta.* 43 (1998) 3141.

186. A. A. Tanaka, C. Fierro, D. A. Scherson and E. B. Yeager, *Mater. Chem. Phys.* 22 (1989) 431

187. V. S. Bagotzky, M. R. Tarasevich, K. A. Radyushkina, O. A. Levina and S. I. Andrusova, *J. Power Sources* 13 (1977) 233

188. J. A. R. vanVeen, J. F. van Baar and K. J. Kroese, *J. Chem. Soc. Faraday. Trans. I,* 77 (1981) 2827

189. D. Scherson, S. L. Gupta, C. Fierro, E. B. Yeager, M. E. Kordesch, J. Eldridge, R. W. Hoffman and J. Blue, *Electrochim. Acta* 28 (1983) 1205

190. D. Scherson, A. A. Tanaka, S. L. Gupta, D. Tryk, C. Fierro, R. Holze and E. B. Yeager, *Electrochim. Acta* 31 (1986) 1247

191. T. Sawaguchi, T. Itlabashi, T. Matsue and I. Uchida, *J. Electroanal. Chem.* 279 (1990) 219

192. A. Widelov and R. Larson, *Electrochim. Acta* 37 (1992) 187

193. M. Ladoucear, G. Lalande, L. Dignard-Bailey, M. L. Trudeau, R. Schulz, D. Guay and J. P. Dodelet, *J. Electrochem. Soc.* 140 (1993) 1974

194. Rongzhong Jiang and Deryn Chu, *J. Electrochem. Soc.* 147 (2000) 4605

195. G. Faubert, G. Lalande, R. Cote, D. Guay, J. P. Dodelet, L.T. Weng, P. Bertrand and G. Denes, *Electrochim. Acta* 41 (1996) 1689

196. G. Lalande, G. Faubert, R. Cote, D. Guay, J. P. Dodelet, L.T. Weng and P. Bertrand, *J. Power Sources* 61 (1996) 227

197. S. Lj. Gojkovic, S. Gupta and R. F. Savinell, *J. Electrochem. Soc.* 145 (1998) 3493

198. S. Lj. Gojkovic, S. Gupta and R. F. Savinell, *J. Electroanal. Chem.* 462 (1999) 63

199. Hendrik Schulenburg, Svetoslav Stankov, Volker Schunemann, Jorg Radnik, Iris Dorbandt, Sebastian Fiechter, Peter Bogdanoff and Helmut Tributsch, *J. Phys. Chem.* B 107 (2003) 9034

200. Ch.Venkateswara Rao and B.Viswanathan (Unpublished results)

201. H. Wang, R. Cote, G. Faubert, D. Guay and J. P. Dodelet*, J. Phys. Chem.* B 103 (1999) 2042

202. G. Faubert, R. Cote, D. Guay, J. P. Dodelet, G. Denes, C. Poleunis and P. Bertrand *Electrochim. Acta* 43 (1998) 1969

203. R. Cote, G. Lalande, G. Faubert, D. Guay, J. P. Dodelet and G. Denes*, J. New Materials for Electrochemical Systems* 1 (1998) 7

204. G. Lalande, R. Cote, D. Guay, J. P. Dodelet, L. T. Weng and P. Bertrand, *Electrochim. Acta* 42 (1997) 1379

205. M. C. Martins Alves, J. P. Dodelet, D. Guay, M. Ladouceur and G. Tourillon, *J. Phys. Chem* 96 (1992) 10898

206. R. W. Joyner, J. A. R van Veen and W. M. H. Sachtler, *J. Chem. Soc. Faraday. Trans.* I, 78 (1982) 1021

207. B. van Wingerden, J. A. R. van Veen and C. T. J. Mensch, *J. Chem. Soc. Faraday. Trans.* I, 84 (1988) 65

208. A. Nath, N. Kopelev, S. D. Tyagi, V. Chechersky and Y. Wei, *Materials Letters* 16 (1993) 39

209. H. J. Choi, G. Kwag and S. Kim, *J. Electroanal. Chem.* 535 (2002) 113
210. M. Lefevre, P. Bertrand and J. P. Dodelet, *J. Phys. Chem* B 104 (2000) 11238
211. M. Lefevre, P. Bertrand and J. P. Dodelet, *J. Phys. Chem.* B 106 (2002) 8705
212. M. Lefevre, P. Bertrand and J. P. Dodelet, *Electrochim. Acta* 48 (2003) 2749
213. M. Lefevre, J. P. Dodelet and P. Bertrand, J. *Phys. Chem.* B 109 (2005) 16718
214. J. Ulstrup, *J. Electroanal. Chem.* 79 (1977) 191
215. F. Beck, *J. Appl. Electrochem.* 7 (1977) 239
216. Ch. VenkateswaraRao and B. Viswanathan, *Indian J. Chem. Sec. A: Inorganic, Bio-inorganic, Physical, Theoretical & Analytical Chemistry*, 43A (2004) 2333.
217. G. Lalande, R. Cote, G. Tamizhmani, D. Guay, J. P. Dodelet, L. Dignard-Baley, L. T. Weng and P. Bertrand, *Electrochim. Acta.* 40 (1995) 2635.
218. S. Gupta, D. Tryk, I. Bae, W. Aldred and E. Yeager*, J. Appl. Electrochem.* 19 (1989) 19
219. R. Jiang and D. Chu, *J. Electrochem. Soc.* 147 (2000) 4605
220. P. Convert, C. Coutanceau, P. Crouigneau, F. Gloagen and C. Lamy, *J. Appl. Electrochem.* 31 (2001) 945
221. S. Gupta, D. Tryk, S. K. Zesevic, W. Aldred, D. Guo and R. F. Savinell, *J. Appl. Electrochem.* 28 (1998) 673
222. G.-Q. Sun, J.-T. Wang, S. Gupta and R. F. Savinell, *J. Appl. Electrochem.* 31 (2001) 1025
223. C. K. Chang, H. Y. Liu and I. Abdalmuhdi, *J. Am. Chem. Soc.* 106 (1984) 2725
224. A. Biloul, O. Contamin, G. Scarbeck, M. Savy, B. Palys, J. Riga and J. Verbist, *J. Eletroanal. Chem.* 365 (1994) 239
225. M. Bron, S. Fiechter, M. Hilgendorff, P. Bogdanoff and S. Fiechter, *J. Eletroanal. Chem.* 32 (2002) 211
226. A. Etcheberry, J. Gautron and J. L. Sculfort, *J. Electroanal. Chem.* 247(1988) 265
227. J. Giner and L. Swette, *Nature* 211 (1966) 1291
228. F. Mazza and S. Trasatti, *J. Electrochem. Soc.* 110 (1963) 847
229. Jan W. M. Jacobs and Jan M. G. Rikken, *J. Electroanal. Chem.* 258 (1989) 147
230. B. Fotouhi and R. Triboulet M. Etman, *J. Electroanal. Chem.* 195 (1985) 425
231. M. Voinov, D. Buehler and H. Tannenberger, *J. Electrochem. Soc.* 118 (1971) 1137
232. A. Vossen, D. R McIntyre, G. T. Burstein, Proceedings - Electrochemical Society (2001), 2001-4(Direct Methanol Fuel Cells), 71
233. K. Lee, A. Ishihara, S. Mitsushima, N. Kamiya and Ken-ichiro Ota, *Electrochim. Acta* 49 (2004) 3479